Pushing and Sliding Allotropes of Carbon

Master internship
Theory of Condensed Matter
Radboud University Nijmegen

Under the scientific supervision of
Drs. M. M. van Wijk
Prof. dr. A. Fasolino

External advisor
Dr. ir. G. de Wijs

by Maria Patelkou

September 20, 2013

Acknowledgements

From all the five years of study, the last has been the most fun, fascinating and educational one for me. I had the luck to be surrounded by very inspiring, intelligent and caring people who taught me a lot about life, research in physics and about myself.
First of all, I want to thank my supervisors Merel van Wijk and Annalisa Fasolino who guided me through my master internship last year.
Merel was my first point of contact when I got stucked with computer programmes and my research in general. You've shown me a lot about molecular dynamics simulations, LAMMPS, awk (programming in general) and how to stay calm in times of stress. I will miss our running sessions through the parks and forests around the university!
I want to thank Annalisa for proposing this research and directing it into the right channels. You taught me a lot about scientific writing, condensed matter theory, empirical potentials and that one should pursue the goals that make one happy. I admire you for your achievements in science, therefore it has been an honour for me to work with you.
Furthermore, I want to thank all members of the "Theory of Condensed Matter"-group for the nice conversations during the breaks, so thank you Koen, Linde, Lennert, Erik, Guus, Jonas, Frank, Remko, Inka, Anja, Timur, Andrea, Shengjun, Misha Titov and Misha Katsnelson. Especially, I want to thank Lennert for helping me out with errors in my C/C++-code and for useful comments and suggestions to improve it.
My study years would not have been so awesome, if it hadn't been for my friends and fellow students here in Nijmegen! I thank Annelot, Rosa, Moniek, Irina, Gijs, Lars, Jan, Alexander, Guus and Tijs for all the nice activities, nights out, house parties, study sessions and lunch breaks. Especially I want to thank Annelot for cheering me up and motivating me when I had a hard time orientating and finding a job. You are a great friend and I am lucky to have you.
Thanks also to my friends in Cologne for the nights out, Starbucks coffies, shopping tours and birthday parties, especially to Kathi who knows me for years and is like a sister to me!
I thank my younger brother Vangeli for all the fun conversations on the phone. We can talk about everything and anything, and understand one another without a lot of words. I am very proud of being your sister!
My biggest thanks go to my parents Georgios and Christina. You raised me, you educated me and you supported me in any possible way. Thanks to you I became the person I am today. I love you a lot!
Last but not least, I want to thank my boyfriend Peter and his family for all their support and love during the last four years. Peter, you are great and I love you a lot!

Contents

1 Introduction

1.1 Sliding friction and wear

Friction is a common phenomenon known from everyday life. It leads to the suppression of the motion of two surfaces in contact. A good example for this is standing. Without friction forces our feet would not stick to the floor. The friction is low for smooth floors and the probability of slipping high.

Most of the time, static friction is a desirable effect. Friction can also arise when solid surfaces are moved with respect to each other. This example falls under the category of kinetic friction, in particular sliding friction.

There are many other forms of kinetic friction like rolling friction for the suppressed motion of rolling solids. In general, the friction between solid surfaces without a fluid lubricant in between is referred to as dry friction.

One can also distinguish friction between layers of viscous fluids (fluid friction), between solid surfaces separated by a fluid (lubricated friction), between a fluid with a solid surface or "skin" (skin friction) and friction between elements in a solid material as its shape undergoes a deformation (internal friction).

Through the motion or deformation of a physical object, mechanical energy is partly converted irreversibly into heat. Basically, this is what friction does to the system. One could interpret this conversion as an energy loss. Therefore, friction does not have only desirable effects. Due to the fact that mechanical energy cannot be fully exploited, it has been estimated that the annual gross national product in the USA results into a loss of 6% which corresponds to 420 billion dollars [1].

The concept of friction in simplified terms is introduced in our educational system early, but most times it is ignored when solving physical problems.

To move or deform physical objects visible with the naked eye, forces are needed. On the macroscopic scale two fundamental forces become important: the electromagnetic and gravitational forces. At the subatomic scale, one should consider not only electric contributions but also the interaction between all kinds of leptons and quarks that seem to become crucial. Additional fundamental forces come into play. However, they have little or no effect on the equations of motion of all electrons and nuclei in the system.

Despite this complexity, friction at the macroscopic scale can be described phenomenologically by simple rules, which have been discovered and rediscovered several times starting from Leonardo da Vinci and now go under the name of Coulomb or Amontons. They can be summarized briefly as follows. To put a body into motion, the frictional force F has to be overcome which is proportional to the load L which often is simply the weight of the body. Equation 1 describes the just mentioned relation where μ is

the proportionality constant that is specific for the surfaces in contact and an eventual lubricant inbetween.

$$F = \mu L \tag{1}$$

The friction force is independent both of the contact area of the surfaces and the surface roughness. It is easier to keep a body in motion than to put it into motion. The kinetic friction force μ_k is smaller than the static friction force μ_s. Normally, the friction force does not depend on the sliding velocity. Only for the case of viscous friction, it depends linearly on the sliding velocity [17].

Recently, thanks to new surface sensitive techniques, the study of friction at the atomic scale is subject of much research in physics with the aim of understanding the fundamental laws leading to energy dissipation and relate them to the behaviour observed at the macroscopic scale. Here we approach this problem from an atomistic point of view, describing the interactions between atoms by means of classical potentials.

The Hamiltonian needed for the integration of the equations of motion depends on all kinetic and potential energy operators of the electrons and nuclei which appear due to their Coulombic attraction and repulsion.

To find the energy of a system in a certain state, the Hamiltonian has to act on this state described by a wave function. This is the well-known Schrödinger equation which can be only solved exactly for small systems like the hydrogen atom. For the description of larger systems approximations are needed. The friction problem is complicated and not well-understood at the atomic scale. It thus deserves a deeper study.

For a long time, the theoretical study of sliding friction seemed to be of interest only for engineering and not for physics. Through the new developments in nanotechnology mentioned earlier, experimental data could be provided which extended this research area to the atomic scale. Especially the inventions of new scanning probe microscopy types like the Atomic Force Microscope (AFM) opened the way for the research area of nanotribology (derived from the Greek words νάνος,"dwarf" and τριβή, "friction") [2].

The focus of this master thesis lies on sliding friction and wear. What is the effect of pushing solid surfaces together and moving them with respect to each other? How can the effect be analyzed? There is a broad range of choices for solids that are suitable for this study.

One of them is diamond which turns out to be a useful abrasive material. It enables the slicing and polishing of all kinds of solid materials. There are many polishing methods that make use of different tools. One option is to use grinding wheels. They are made of diamond particles on metal discs, mostly made of iron or steel. Such a metal disc is rotated at a speed of roughly 30 m/s and pushed against the surface of the solid material. The polishing of diamond with diamond grinding wheels has been done already

for hundreds of years.

Craftsmen have come to realize that polishing of certain diamond surfaces along certain directions leads to more resistance than for others. When polishing under resistive conditions, the resulting surface is rough and worn out. This circumstance has been studied scientifically and one has come to the conclusion that wear in diamond depends on the crystallographic surface and the direction along which it is polished.

The wear of diamond is high when polishing the (100) and (110) surfaces along the <110> direction, and any other surface along the <111> direction. The wear is low when polishing the (100) and (110) surface along the <100> direction.

To explain this phenomenon one assumed in the beginning, that small diamond crystals detach from the surface due to the abrasion, a process called wear. Thanks to advanced microscopic techniques, one succeeded quite recently in detecting a thin layer of amorphous carbon on a nanocrystalline diamond surface after polishing it [3]. Lars Pastewka et al.[4] carried out a molecular dynamics simulation of two diamond surfaces that are pushed together and moved with respect to each other. The aim was to understand the finding of the earlier carried out experiment which is the occurrence of amorphous particles, and their microscopic origin. Their results are presented in fig.1.

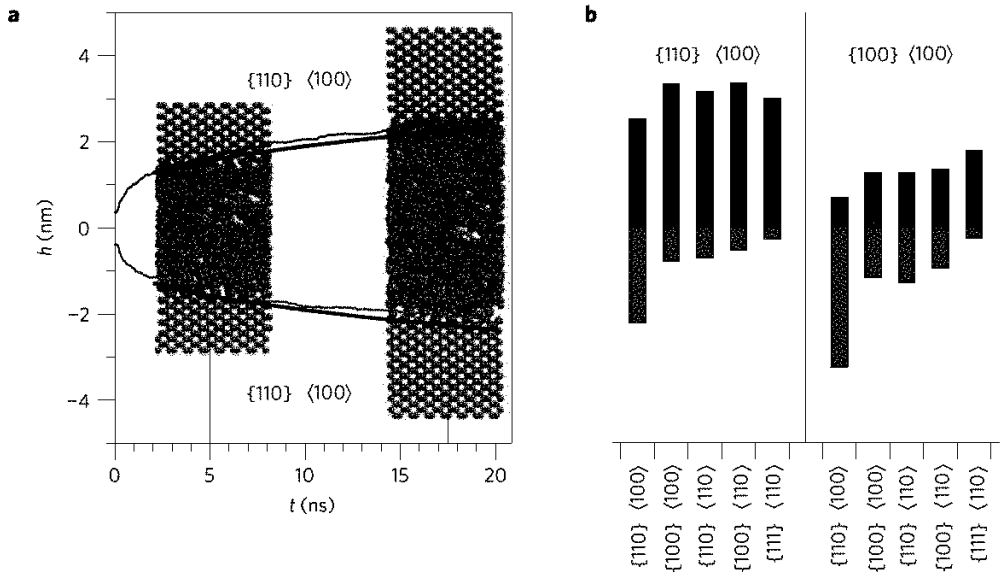

Figure 1: a) The formation of the amorphous layer between two (110) surfaces that are polished in the <100> direction is shown as a function of time in nanoseconds. The thickness of the amorphous layer is shown on the vertical axis in nm. b) The thickness of the amorphous layers for various combinations of surfaces and directions are presented after 20 ns.[4]

Pastewka et al. suggested a simulation in which both bulk structures are pushed together at 10 GPa, equilibrated and then the top rigid layer starts to move at a constant velocity of 30 m/s. The bond-order potential that is used in their simulation to describe carbon-carbon interatomic interactions is the reactive empirical bond-order potential (REBO).

In this thesis, it is tried to reproduce this molecular dynamics simulation with the difference that the bond order potential used in our simulation is the long-range order carbon bond order potential (LCBOB). The simulation is not only carried out with diamond structures. We want to go a step further and study the effect of pushing and sliding the different allotropes of carbon which are introduced in the following section.

Thanks to the molecular dynamics simulations it is possible to follow the trajectories of the atoms. A huge amount of data can be generated with information on various atomic properties. The processing of raw data enables new insights of the effect on the atoms at the interface due to pushing and sliding. Different analysis methods are applied on the system to study the formation of amorphous carbon (see section 4). The aim of this master thesis is to carry out molecular dynamics simulations of pushing and sliding different allotropes of carbon bulk structures and to analyze the formation and the structure of the interface.

1.2 Allotropes of carbon

Carbon is a unique element. Its element number is six which means that carbon has six electrons. Its electronic configuration is $1s^2 2s^2 2p^2$ where 1s, 2s and 2p stand for the atomic orbitals in which the electrons are distributed pairwise. As carbon has only six protons and six neutrons, its atomic mass number is 12 and therefore, it is one of the lightest elements in the periodic table.

This has consequences for the lattice parameter of the cubic cell of diamond. Compared to the cubic diamond structure of silicon and germanium, diamond has a much smaller lattice parameter (see table 1).

Material	Lattice parameter in Å at 300K	Electronic configuration
Diamond	3.56683	$1s^2 2s^2 2p^2$
Silicon	5.43095	$1s^2 2s^2 2p^6 3s^2 3p^2$
Germanium	5.64613	$1s^2 2s^2 2p^6 3s^2 3p^6 4s^2 3d^{10} 4p^2$

Table 1: The lattice parameters in Å at 300K and the electronic configuration for diamond, silicon and germanium.

At first sight, it is quite surprising that carbon can take different forms. If one assumed that the two s-orbitals are filled and only the two electrons in the exterior 2p-orbital can form covalent bonds, carbon would be just divalent. Carbon would form two bonds and would exist only in linear chains. But this is the case only for small clusters up to 20 atoms[14].

Carbon can be also tetravalent or trivalent, thus form four or three covalent bonds as a consequence of the formation of hybridized sp-orbitals where also two electrons in the 2s-orbital contribute to the covalent bond formation.

In diamond, each carbon atom has four covalent electrons and is thus bonded to four other carbon atoms. It is known as a strong bulk material with the highest hardness. It is not conducting due to the fact that all valence electrons are bonded and localized in pairs between the atoms.

Another well known three-dimensional allotrope of carbon is graphite. It is built out of multiple graphene layers where the carbon atoms are bonded to three other atoms and form a hexagonal lattice (see section 5.2.3). The fourth electron is delocalized and can move freely through the whole crystal and give rise to a kind of van der Waals interaction between the graphene layers. Graphite is therefore an electrical conductor in the plane.

Within the layer, the bonds are very strong whereas the bonds between the layers are weak. The layers are held together through van der Waals forces.

For a long time it was believed that a two-dimensional material like

graphene could not exist in reality. The scientific breakthrough by Andre Geim en Konstantin Novoselov proved the opposite. They succeeded in isolating a single hexagonal layer of carbon, graphene. As the bonds between the layers in graphite are weak, single layers can be removed by applying scotch tape on it. The graphene flakes stick on the tape and can then be deported on a silicon wafer.

By the scotch-tape-method, one can produce up to 3 mm by 3 mm monocrystalline graphene flakes. The price per gram is 10^{15}€, a huge price because a square meter of graphene weighs 0.77 milligrams. For diamond, the price per gram can be 70.000€ at maximum. The production of graphene through the exfoliation method is thus even more expensive than diamond.

To describe the crystals, the following notation is used. Unit cells are described by lattice vectors. In three-dimensional systems, there are three lattice vectors $\mathbf{a}_1$, $\mathbf{a}_2$ and $\mathbf{a}_3$. Taking these three vectors together and translating them over the whole space, leads to a three-dimensional crystal structure. For a two-dimensional structure, one needs two lattice vectors.

Within the elementary cell, atoms can be placed. They form the basis of the lattice and are described by the vector $\boldsymbol{\delta}_j$. The index j labels the atoms in the elementary cell.

The following formula describes in general the filling of the whole space by the i=0,1,...,N cells each containing j=0,1,...,n atoms where n_1, n_2 and n_3 are integer numbers.

$$\mathbf{R}_{i,j} = n_1\mathbf{a}_1 + n_2\mathbf{a}_2 + n_3\mathbf{a}_3 + \boldsymbol{\delta}_j \tag{2}$$

In the following sections, several allotropes of carbon are introduced and described using this notation.

1.2.1 Graphene

The carbon atoms in graphene are arranged in a two-dimensional hexagonal crystal structure.

There are j=2 atoms in the basis with $\boldsymbol{\delta}_1$=(0, 0, 0) and $\boldsymbol{\delta}_2$=(2a, 0, 0), where a is the interatomic distance. The lattice vectors in graphene are given by $\mathbf{a}_1$=a/2(3, $\sqrt{3}$, 0), $\mathbf{a}_2$=a/2(3, -$\sqrt{3}$, 0) (see formula 2).

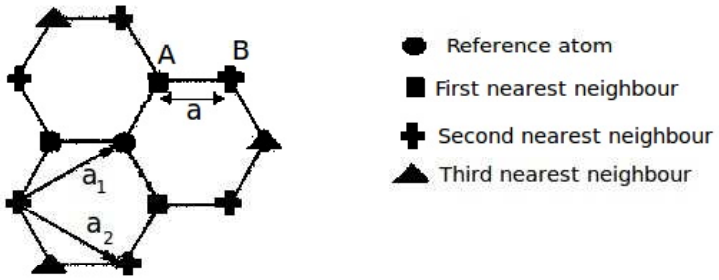

Figure 2: Illustration of the lattice vectors $\mathbf{a}_1$ and $\mathbf{a}_2$ and the three first nearest neighbour atoms at distance a=1.42 Å from the reference atom, six second nearest neighbour atoms at $\sqrt{3}a$=2.45 Å and the three third nearest neighbour atoms at $2a$=2.84 Å.

In fig.3, the total energy per atom as a function of interatomic distance a is shown. For the calculations, the classical molecular dynamics code LAMMPS (see section 3.5.1) and the empirical potential LCBOP is used (see section 3.2). There is a minimum at a=1.42 Å indicating that this is the optimal interatomic distance for which the total energy per atom is in its minimum. The plot does not follow a perfect parabola around the minimum, because the LCBOP potential accounts also for anharmonic interactions.

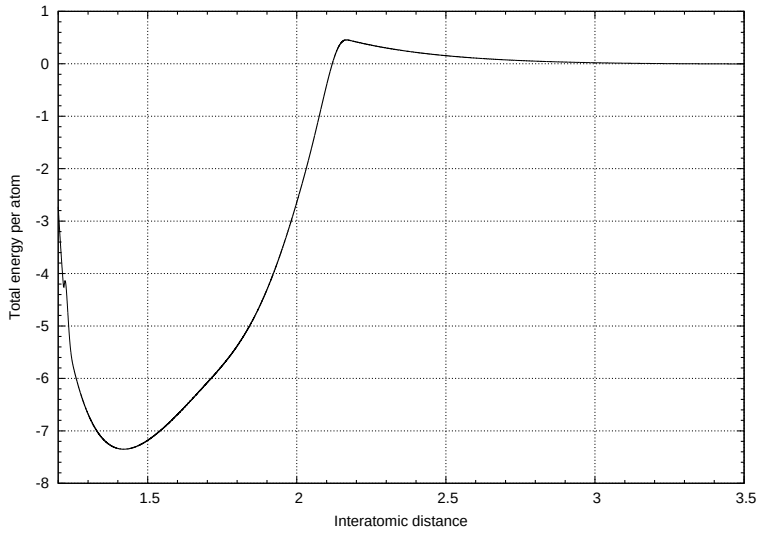

Figure 3: Total energy per atom (in eV) as a function of the interatomic distance a (in Å) in the interval from 1.2 Å to 3.5 Å. There is a minimum at 1.42 Å at -7.35 eV.

Another feature of fig.3 is the maximum energy at 0.46 eV at the interatomic distance 2.2 Å. From that point on, the energy per atom is slowly

decreasing and has a second minimum at 3.34 Å. As shown in fig.4, the covalent short range interactions are cut off at 2.2 Å in the LCBOP potential.

The long tail in fig.3 will be examined more carefully in fig 5.

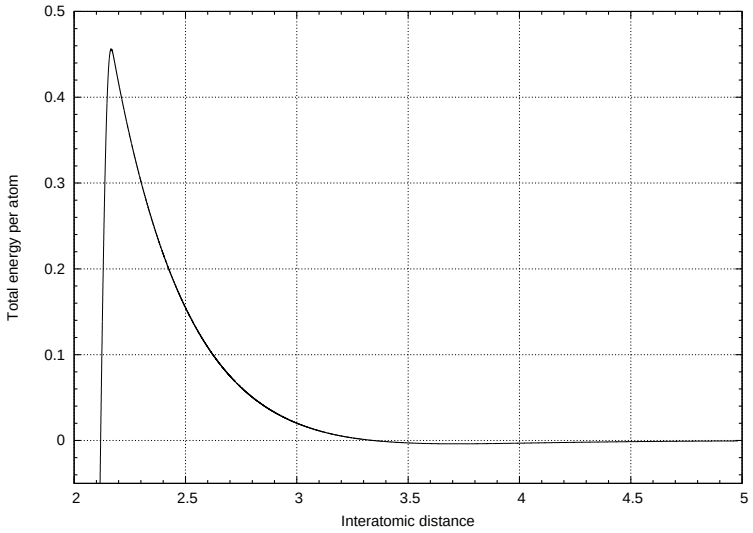

Figure 4: Total energy per atom (in eV) as a function of the interatomic distance a (in Å) in the interval from 2.0 Å to 5 Å showing the maximum energy 0.46 eV at the interatomic distance 2.2 Å and the change of the slope.

In fig.5 the energy per atom is examined from 3.3 Å to 7 Å. At 3.72 Å, there is another minimum of the energy with the value -39.3 meV. The behaviour of the total energy beyond the cut off distance 2.2 Å of the covalent bonding is due to the way chosen in LCBOP to include longe range terms that account for the weak interactions in graphite.

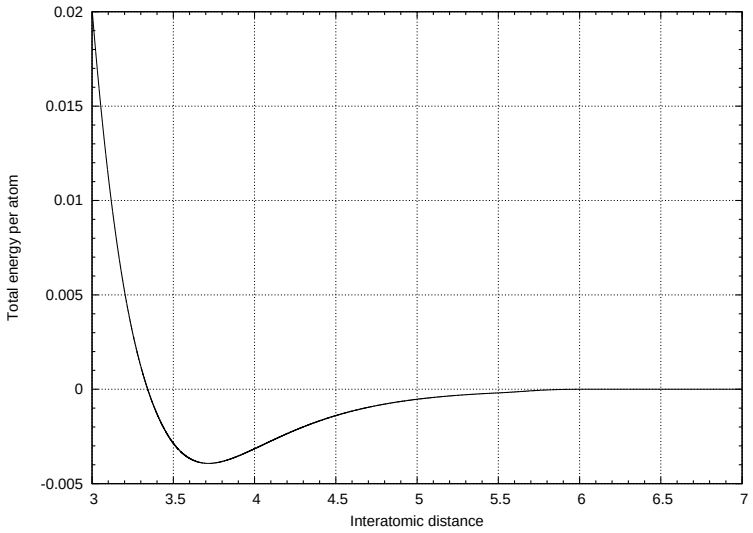

Figure 5: Total energy per atom (in eV) as a function of the interatomic distance a (in Å) in the interval from 3 Å to 7 Å showing another minimum at 3.52 Å with the energy -39.3 meV.

1.2.2 Graphite

Graphite consists of multiple graphene layers. There are several ways to stack graphene layers on top of each other. The most common and energetically stable stacking is the AB Bernal stacking where the second layer is rotated by 60 ° with respect to the first one.

Placing a third layer on top of that rotated again by 60 ° leads to the rhombohedral stacking, also known as the ABC stacking.

Constructing the layers one on top of another without any rotation is called AA stacking. There, the lattice vectors are just as in graphene with the difference that a third vector a_3=(0, 0, c) is added that creates exactly the lattice at a distance c from the first layer, without any rotation, where c is the interplanar distance. The basis atoms are placed at the same positions as for graphene.

Next, the distance c between two layers in the AA stacking is varied from 2.8 Å to 8 Å and the total energy per atom is calculated. The result is presented in fig.6.

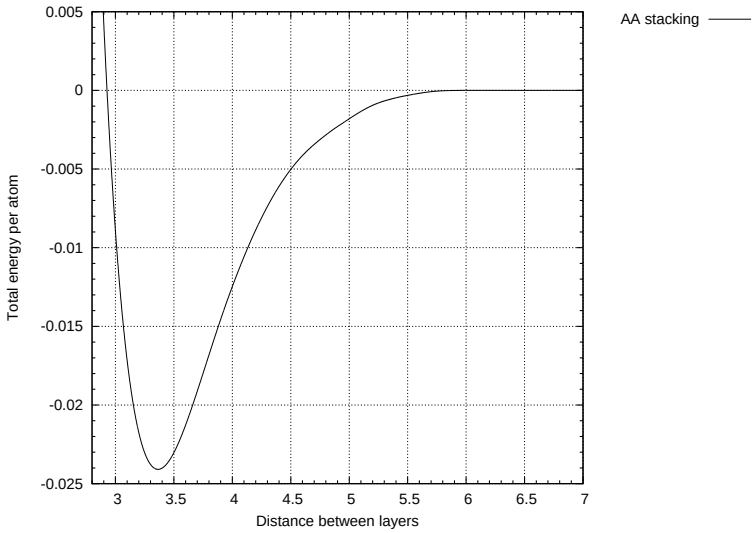

Figure 6: Total energy per atom (in eV) as a function of the interlayer distance (in Å) in the interval from 2.8 Å to 8 Å for the AA case. There is a minimum in the total energy per atom for 3.36 Å at -24.01 meV.

The minimum energy for the AA stacking occurs at 3.36 Å at -24.09 meV.

In the following, the AB Bernal stacking is explained. In this case, the periodicity along z is $2c$ meaning that the A-layers are separated by that distance. The unit cell is described by the two lattice vectors that are introduced for graphene in section 1.2.1 and a third vector a_3=(0, 0, $2c$). The four basis atoms placed at the positions δ_1=(0, 0, 0), $\boldsymbol{\delta}_2$=($2a$, 0, 0), $\boldsymbol{\delta}_3$=(a, 0, c) and $\boldsymbol{\delta}_4$=($3a$, 0, c) (see formula 2). In fig.7, the crystal structure of graphite in the AB Bernal stacking is presented from above and sidewards.

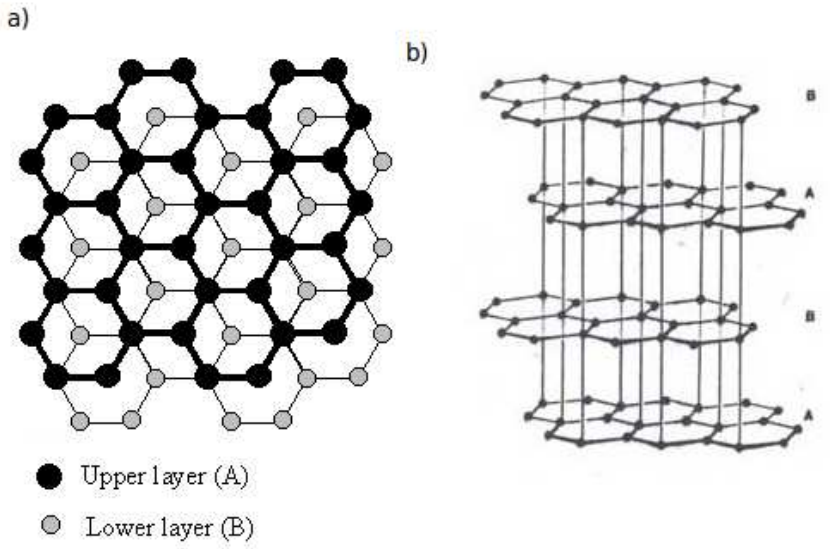

Figure 7: Arrangement of carbon atoms in graphite in the AB Bernal stacking consisting of two layers A and B shown from a) above and b) sidewards.

Next, the distance c between two AB layers is varied from 2.8 Å to 7 Å and the total energy per atom is calculated. The result is presented in fig.8. There is a minimum in the energy at 3.35 Åindicating the optimal interlayer distance for graphite in the AB Bernal stacking.

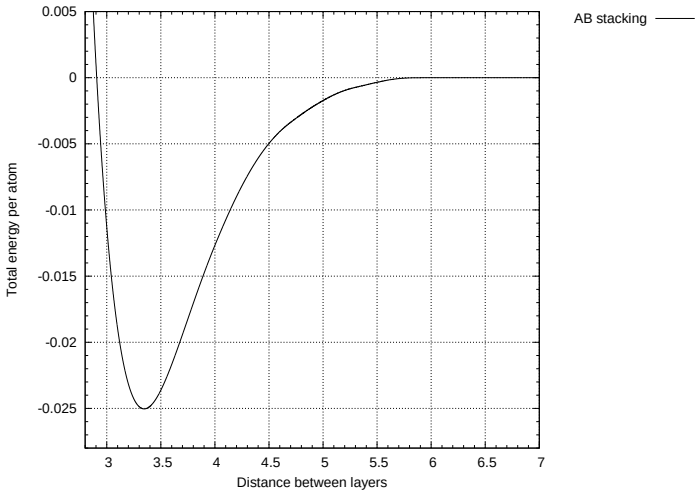

Figure 8: Total energy per atom (in eV) as a function of the interlayer distance (in Å) in the interval from 2.8 Å to 7 Å for the AB stacking. There is a minimum in the total energy per atom for 3.35 Å at -25.03 meV.

Next, the ABC rhombohedral stacking is explained. The periodicity along z is $3c$. The unit cell is described by the two lattice vectors introduced for graphene in section 1.2.1 and a third vector a_3=(0, 0, $3c$). There are six basis atoms that are placed at the positions $\boldsymbol{\delta}_1$=(0, 0, 0), $\boldsymbol{\delta}_2$=($2a$, 0, 0), $\boldsymbol{\delta}_3$=(a, 0, $1/3c$), $\boldsymbol{\delta}_4$=($3a$, 0, $1/3c$), $\boldsymbol{\delta}_5$=($2a$, 0, $2/3c$), $\boldsymbol{\delta}_6$=($4a$, 0, $2/3c$) (see formula 2).

The the distance between two ABC layers is varied from 1 Å to 7 Å and the total energy per atom is calculated. The result is presented in fig.9. There is a minimum at 3.35 Å indicating that the graphite in the ABC stacking is in its energetic equilibrium at this distance between the layers.

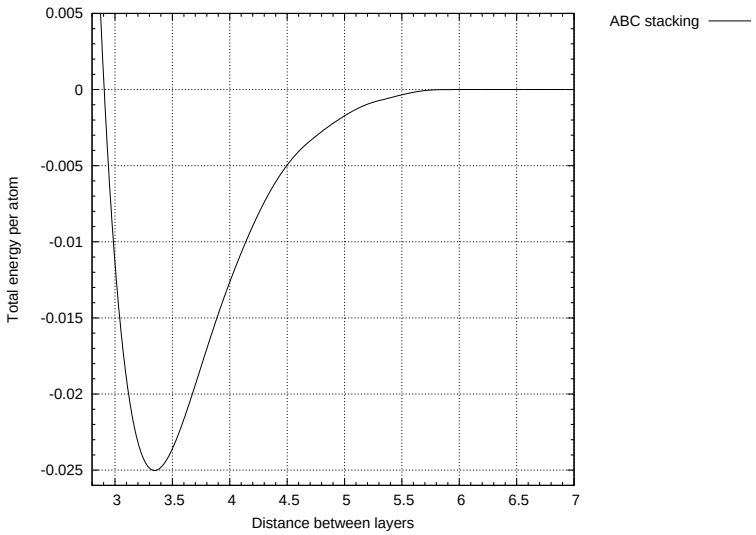

Figure 9: Total energy per atom as a function of the layer distance za in the interval from 2.8 Å to 7 Å for the ABC case. There is a minimum in the total energy per atom for 3.35 Å at -25.01 meV.

The distance between the energy minima of the AB and ABC stacking is E_{AB}-E_{ABC}=-0.02 meV. This difference is much smaller than the distance between the energy minima of the AB and AA stacking E_{AB}-E_{AA}=-1.02 meV. The most favorable stacking is thus AB, followed by ABC. The AA stacking is the least favorable. The differences in energy become evident in fig.10.

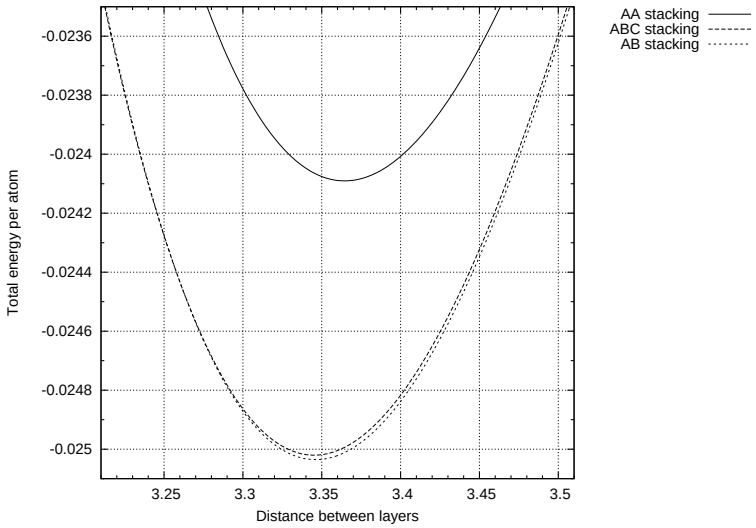

Figure 10: Total energy per atom (in eV) as a function of the interlayer distance (in Å) for the AA, ABC and AB case in the interval from 3.22 Å to 3.52 Å.

1.2.3 Corrugation energy surface of graphite in the AB Bernal stacking

To construct the corrugation energy surface of graphite in the AB Bernal stacking, the second layer B is shifted in x- and y-direction and the pairwise energy per atom is calculated in eV[5]. The pairwise energy is composed of the van der Waals long-range interaction energies between the carbon atoms.

The unit cell that is used here are two layers with 16 atoms in each layer. Periodic boundary conditions are applied in the x- and y-direction. A single layer is depicted in fig.11. In the x-direction, the B-layer is shifted from 0 to 4.24 Å which is roughly three times the lattice parameter a=1.42 Å. In the y-direction, the B-layer is shifted from 0 to 2.45 Å which is $\sqrt{3}a$. By shifting the B-layer over those distances in x- and y-direction, it is possible to construct graphite in different stackings.

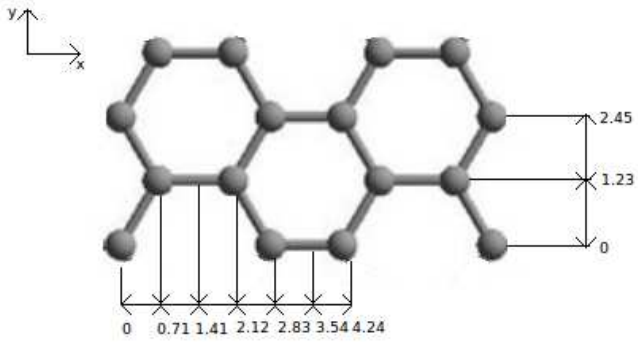

Figure 11: Illustration of the 16-atom unit cell and the corresponding shifts in x- and y-direction indicated by arrows.

If the B-layer is shifted by 2.83 Å in the x-direction and 0 Å in the y-direction, graphite in the AA stacking is achieved. Shifting the B-layer by 4.24 Å in the x-direction and 0 Å in the y-direction brings the graphite structure back to the AB Bernal stacking. Fig.12 illustrates the shifts by 0 Å, 2.83 Å and 4.24 Å in the x-direction.

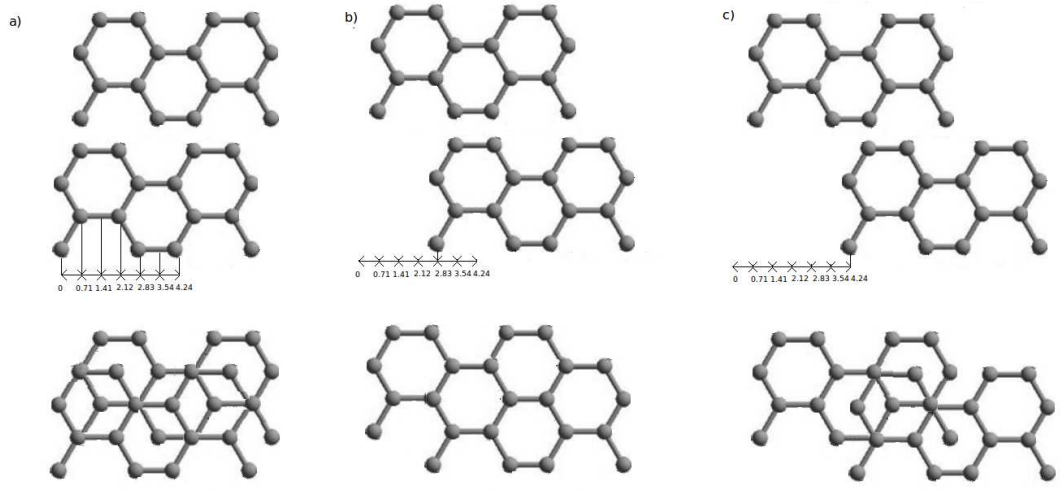

Figure 12: Shift of the B-layer by a)0 Å b)2.83 Å and c)4.24 Å in the x-direction which gives rise to graphite in the a)AB Bernal b)AA and c)AB Bernal stacking. The structures at the top depict how the shift is performed. The structures thereunder illustrate the view from the top.

So for different shifts, graphite in different stackings can be realized. From earlier calculations it is known, that graphite in the AB Bernal stacking is energetically the most favourable structure. For the shifts x=0 Å, y=0 Å and x=4.24 Å, and y=0 Å, there is a minimum in the energy.

Graphite in the AA stacking is energetically the least favorable structure which means that there is a maximum in the energy for x=2.83 Å y=0 Å. The AA-stacking also occurs for the shifts x=2.83 Å,y=2.45 Å and x=0.71 Å, y=1.23 Å so all by all there are three maxima in the corrugation energy surface.

All pairwise energies are calculated with respect to the minimum total energy of graphite in the AB Bernal stacking which is -7.375 eV.

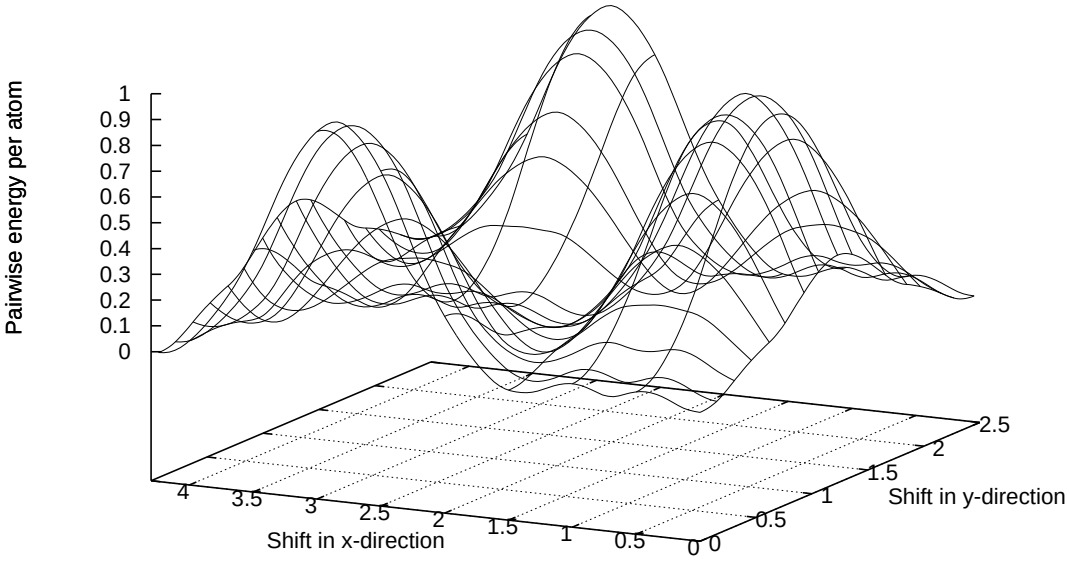

Figure 13: The corrugation energy surface of graphite in the AB Bernal stacking. On the in-plane horizontal axis, the displacement of the B layer in x-direction is shown, and on the vertical axis the displacement of the B-layer in y-direction is displayed (both in Å). On the axis perpendicular to the plane, the pairwise energy per atom in meV is shown.

In the following figure, the pairwise energy per atom is shown for the shift in the x-direction while there is no shift in the y-direction.

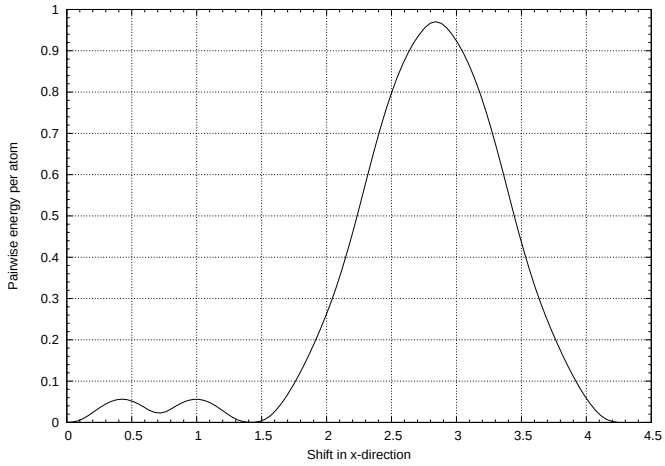

Figure 14: Shift in x-direction (in Å) as a function of the pairwise energy per atom (in meV), while there is no shift in the y-direction. Notice the maximum at the x-shift x=2.83 Å and the minima at x=0 Å x=1.41 Å and x=4.24 Å.

The maximum total energy corresponds to the total energy of graphite in the AA stacking. The minimum total energies correspond to the total energy of graphite in the AB stacking. The difference between the AA and the AB pairwise energy is 0.970 meV.

1.2.4 Corrugation energy surface of incommensurate graphite

Another way to arrange graphene layers in graphite is to rotate the second B-layer by 30 ° with respect to the first layer. This arrangement of graphene layers is also known as incommensurate graphite. The rotation of the second layer gives rise to a special pattern that is called Moiré pattern shown in fig.15.

Moiré-patterns are of great interest in modern physics as they change the periodic potential through which free electrons propagate.

One way to study the electronic properties of for instance monolayer graphene, is to suspend it on a substrate. The most popular substrates for graphene are silicon oxide (SiO_2) and boron nitride (BN). In the end, SiO_2 turned out to be not suitable for graphene as the mobility of the charge carriers was low. However, the mobility is greatly improved when isolating graphene on BN[17].

Using scanning tunneling microscopy, local microscopic properties of graphene on BN has been studied which display indeed Moiré patterns due to the rotation of the lattices with respect to each other[18].

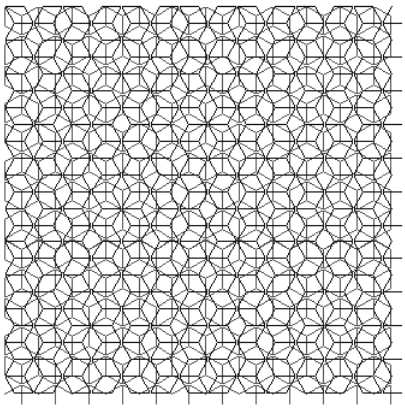

Figure 15: Moiré pattern of incommensurate graphite.

In this section, the corrugation energy surface of incommensurate, also called Moiré-patterned, graphite is constructed. To produce Moiré-patterned graphite, the periodicities of the two layers have to match when building an infinite unit cell. The solution to this problem is discussed in section 2.1.1 where the construction of simulation boxes with periodic boundary conditions in the x- and y-direction containing two different crystal structures is presented.

In fig.16, the corrugation energy surface is shown. Again, the second layer is shifted in the x- and y-direction with respect to the first layer. When comparing the corrugation energy surfaces of incommensurate (fig.16) and commensurate (fig.13) graphite, it strikes that the energy per atom of incommensurate graphite is of the order of micro-electron-volt (10^{-6} eV), whereas for commensurate graphite, it is of the order of milli-electron-volt (10^{-3} eV). From that one could state that incommensurate sliding is less resistant than commensurate sliding. It is easier to slide the second layer if it is rotated by 30 $^{\circ}$ with respect to the first one.

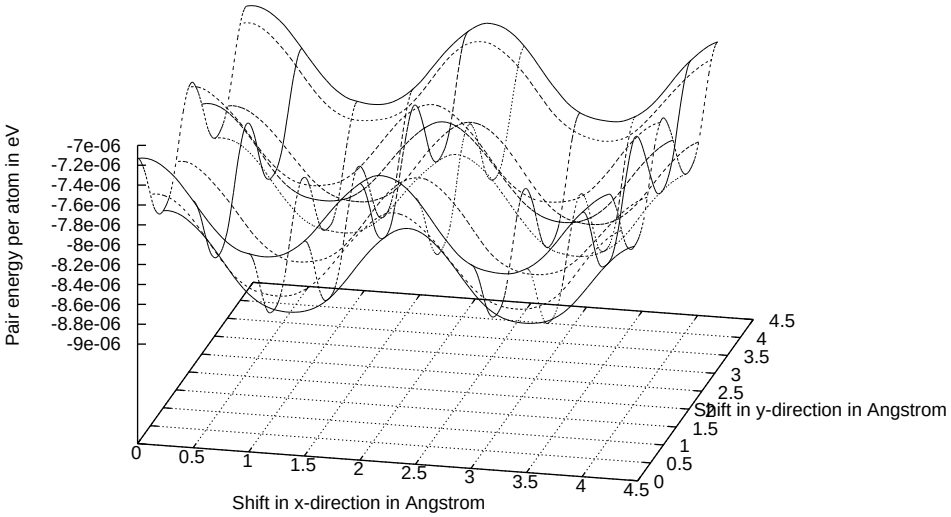

Figure 16: Corrugation energy surface of incommensurate graphite

1.2.5 Diamond

The unit cell in diamond is cubic and described by three lattice vectors $\mathbf{a}_1$=a(0, 1/2, 1/2), $\mathbf{a}_2$=a(1/2, 0, 1/2) and $\mathbf{a}_3$=a(1/2, 1/2, 0) where a is the lattice constant as shown in fig.17a). The two basis atoms are placed at positions $\boldsymbol{\delta}_1$=(0, 0, 0) and $\boldsymbol{\delta}_2$=(1/4a, 1/4a, 1/4a). The interatomic distance in terms of the lattice constant is $\sqrt{3}/4$ a.

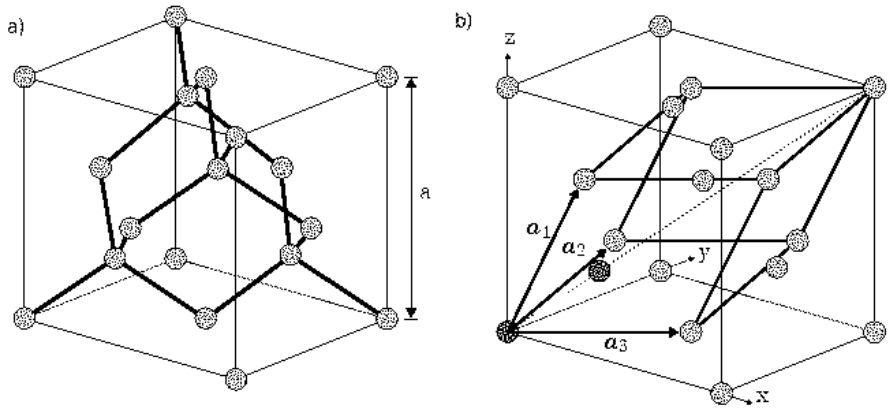

Figure 17: Arrangement of carbon atoms in diamond where a) depicts the bonds between the carbon atoms and b) illustrates the three lattice vectors a_1, a_2 and a_3 as well as the two basis atoms in dark grey.

In fig.18, the total energy per atom is shown as a function of the interatomic distance. There is a minimum in total energy per atom at 1.54 Å. The lattice constant is thus a=3.55 Å.

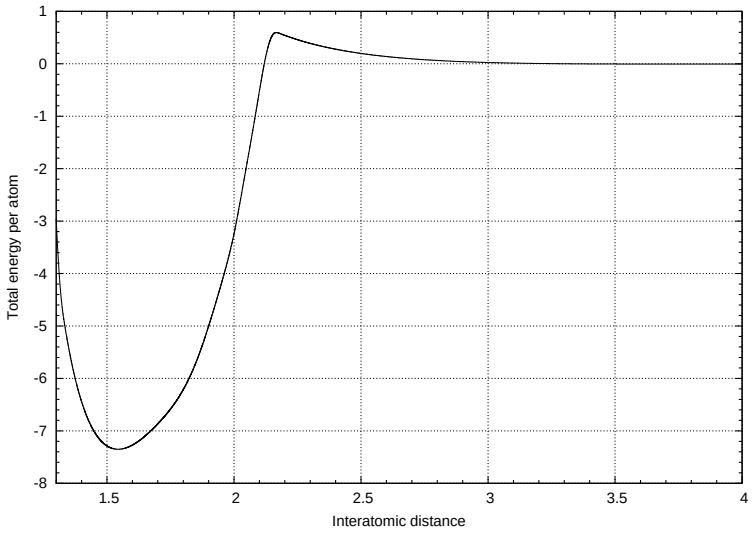

Figure 18: Total energy per atom (in eV) as a function of interatomic distance (in Å) in the interval 1.3 Å to 4 Å. There is a minimum in the total energy per atom at 1.54 Å at -7.35 eV.

The unit cell explained above describes diamond where the (100)-surface is normal to the z-direction. In the simulations of wear that we will show in section 2, the (111)-surface of diamond is considered. Its unit cell is orthogonal and is described by the three lattice vectors $\mathbf{a}_1$=(1.2425, -1.2425,

0), $\mathbf{a}_2$=(1.775, -1.775, 0) and $\mathbf{a}_3$=(1.2425, 1.2425, 2.52). The two basis atoms are placed at (0, 0, 0) and (0.63, 0.63, 0.63).

1.2.6 Amorphous carbon

In amorphous carbon, the carbon atoms are connected by bonds without any long-range order. The number of sp^2 and sp^3 hybridized carbon atoms can vary. The more sp^2 hybridized carbon atoms, the more the amorphous structure has common properties with graphite. The more sp^3 hybridized carbon atoms, the more the the amorphous structure has common properties with diamond. In industry, such a amorphous structure is called "Diamond like carbon" (DLC) where also hydrogen can be present.

In the following, a diamond structure consisting of 128 carbon atoms is used to prepare amorphous carbon. The atoms are displaced randomly by 0.0142 Å(one percent of their interatomic distance) in each direction before the simulation starts.

Then, the carbon structure is kept at 0.1 K for 1ps, then heated up to 7000K in 3ps and kept at that temperature for 3.5ps. This temperature is much higher than the melting temperature of diamond which is 4095 K at atmospheric pressure. At last, it is suddenly cooled down to 10K and kept at that temperature for 1ps. The annealing cycle is presented in fig.19.

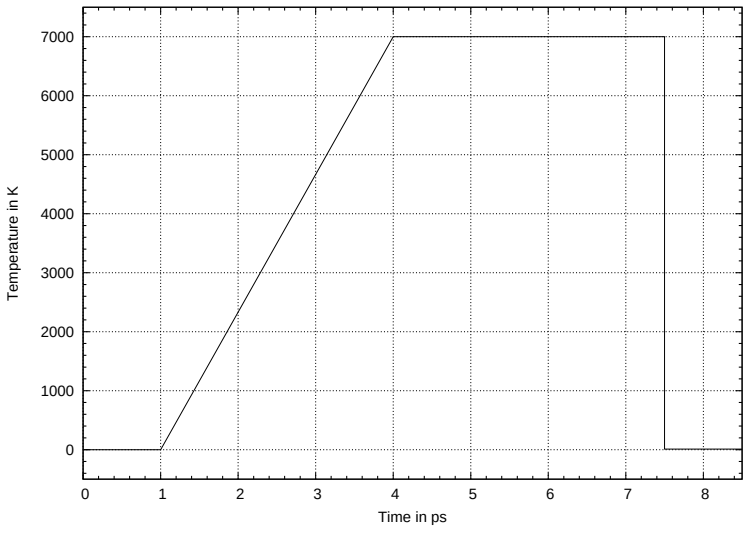

Figure 19: The annealing cycle expressed in temperature as a function of time.

In fig.20, the carbon structures at 7000K and 10K are shown.

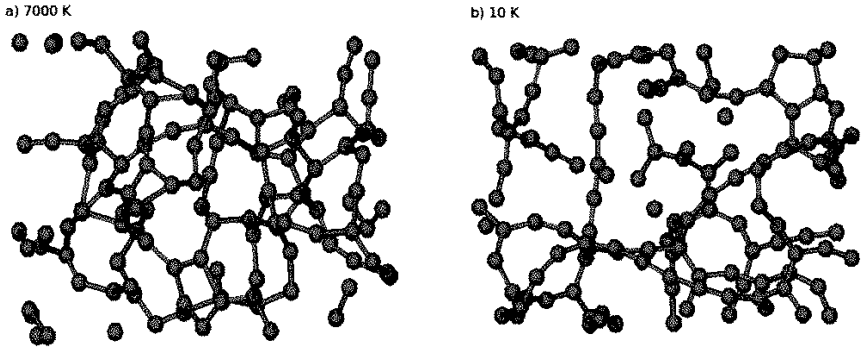

Figure 20: The carbon structure at a)7000K and at b)10 K after the structure is heated up.

The density of the carbon atoms is not constant over the whole space, but varies. By means of the radial distribution function, one can express the probability of finding a particle at a certain distance from another particle. The interatomic distances are binned and averaged over many confirmations as described later on in section 4.1.

In fig.21, the radial distribution function is shown for the carbon structure at 10 K and at 7000 K. At 10 K the first peak is at a distance that spans from 1.2 Å to 1.6 Å, the interatomic distances in different allotropes from linear chains to diamond. At 7000 K the radial distribution function is that of a liquid.

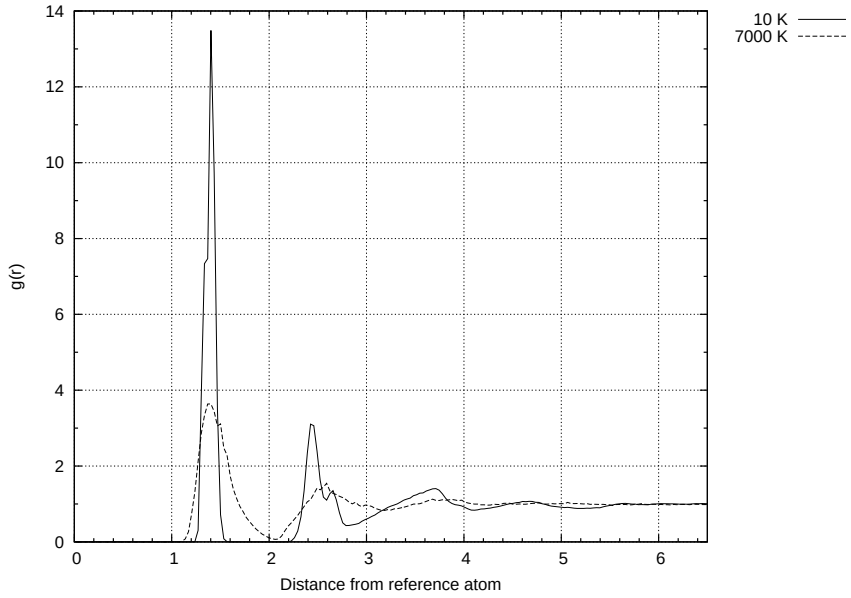

Figure 21: The radial distribution function g(r) of the carbon structure at 10 K and at 7000K as average over 200 bins. A bin is a arrangement of data into classes. In this case a bin represents a class of atoms that are at a certain distance (in Å) from a reference atom.

The coordination number of an atom reveals information on the number nearest neighbours in an atom. If an atom has one nearest neighbor, its coordination number is 1, if it has two, its coordination number is 2, and so on. The maximal distance within which the carbon atoms form a bond is set to 2.2 Å. From that distance on the atoms do not have any short-range interaction with each other. It is also called the cut-off distance at which the short-range part of the LCBOP potential is cut off.

For the carbon structures at 10 K and 7000K, the number of atoms is shown in fig.22 as a function of the coordination number. The coordination number 2 does appear the most for the carbon structure at 10 K, with a number of 68 atoms, followed by the coordination number 3 with a number of 55 atoms. Only 5 atoms have a single nearest neighbor.

For the carbon structure at 7000 K, there are 14 atoms with one nearest neighbor, 51 atoms with two atoms bonded to them and no atoms that are bonded to three atoms. The coordination number 4 appears the most as there are 63 atoms that have four nearest neighbours.

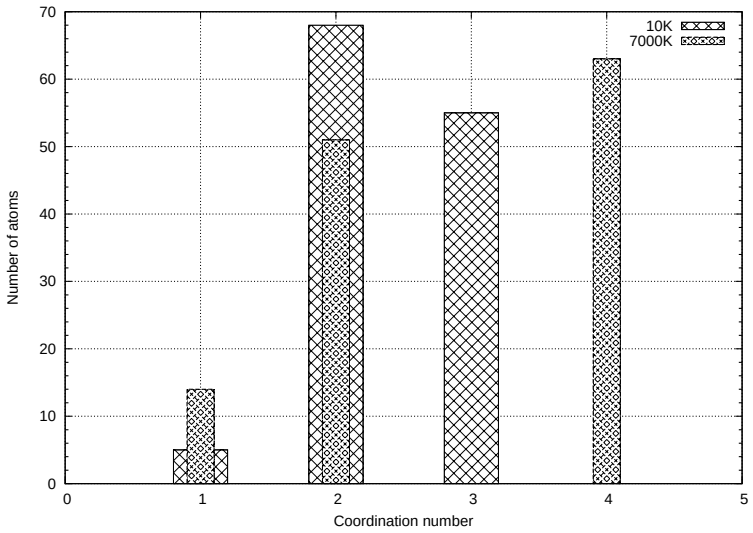

Figure 22: The number of atoms of the carbon structures at 10 K and at 7000 K as a function of the coordination number.

1.2.7 Clathrate

A clathrate is a certain lattice type where atoms seem to be trapped in a cage. It usually consists of two chemical substances. The first substance is called the guest compound as it is trapped in the cage. The other substance is called host or clathrate compound (lat. *clatratus* "lattice, with bars") and represents the cage where the guest compound is trapped.

Although this structure has been experimentally realized in silicon and germanium but not yet in carbon, the latter is predicted to be stable up to high temperatures[15].

There are no guest compounds present in our simulations, just the clathrate. The sample that is used consists of 368 atoms that are placed in an orthogonal box depicted in fig.23.

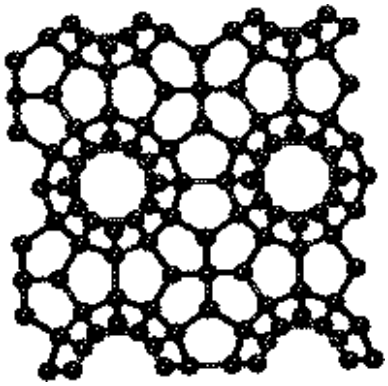

Figure 23: Illustration of the 368 atoms arranged in the clathrate structure.

1.2.8 Low-energy structures

The low-energy structure is produced by a random geometry generator designed by M.A. Akhukov [6]. Its purpose is to generate nanosized, metastable carbon structures which might exhibit magnetic moments. Many of the samples turned out to be diamond or graphite which are low in energy (-7.35 eV/atom and -7.37 eV/atom) and stable. However, there are 414 samples out of the 25000 realizations that have an energy close to diamond and graphite (-7 eV/atom). All samples were relaxed by means of the conjugated gradient algorithm in LAMMPS with the empirical potential LCBOP.

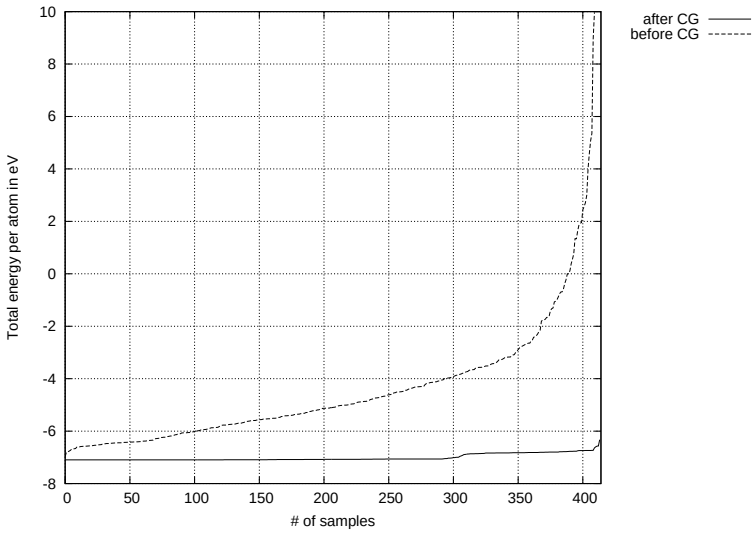

Figure 24: The total energy per atom (in eV) from the low-energy-structures before and after the conjugated gradient relaxation.

Many of the structures became graphite, but some of them remained

stable. The structure that is described here, is one of them. Its energy per atom is -6.8 eV and consists of eight atoms in the unit cell. The unit cell is rotated in such a way that the graphene-like surface is on the top.

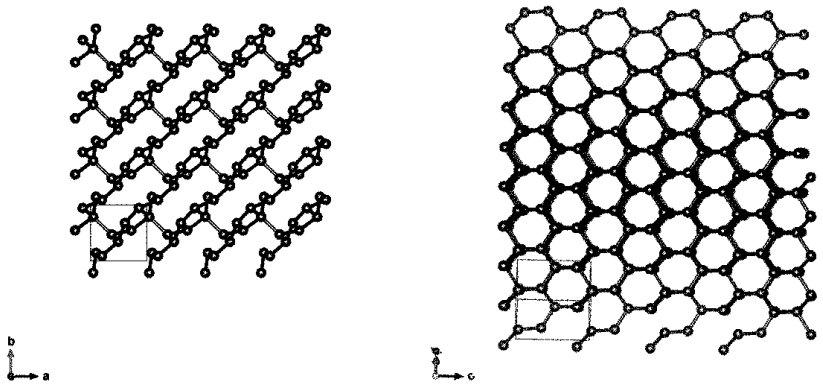

Figure 25: The low-energy structure is rotated in such a way that the graphene-like surface is on the top.

The lattice spacings in the x-, y- and z-direction are 4.685 Å · 4.34409 Å · 4.685 Å.

1.3 Elastic constant

Elastic constants describe the relation between stress and strain in a stretched material. They are characteristic for a material. The greater their value, the more resistance does the material set against stretching.

To describe the physical idea of stretching, Hooke's law is applied. It states that for small deformations of an elastic crystal, the strain is directly proportional to the stress. In formula 3, ϵ represents the extension or strain which is proportional to the stress σ in units of force per area. The constant C in units of force per area (or energy per volume) is the proportionality factor between the stress σ and the dimensionless strain ϵ. It is called elastic constant.

$$\sigma = C\epsilon \tag{3}$$

The strain ϵ can be applied in all three dimensions, therefore it is a 3x3 tensor. It can be expressed in terms of the symmetric stress tensor e, where α is the parameter by which the lattice is distorted.

$$e = \begin{bmatrix} 1+\alpha_{xx} & \alpha_{xy} & \alpha_{xz} \\ \alpha_{yx} & 1+\alpha_{yy} & \alpha_{yx} \\ \alpha_{yz} & \alpha_{zy} & 1+\alpha_{zz} \end{bmatrix}$$

Every crystal is characterized by lattice vectors which can be extended or shortened by a certain lattice distortion parameter, which is called α here. In this method, a uniform deformation of the crystal is considered, that is why α is uniform in each direction. To find the distorted lattice vectors a_1', a_2' and a_3', the strain tensor e is multiplied with each lattice vector a_1=(a_{11}, a_{12}, a_{13}), a_2=(a_{21}, a_{22}, a_{23}) and a_3=(a_{31}, a_{32}, a_{33}).

$$\begin{bmatrix} 1+\alpha_{xx} & \alpha_{xy} & \alpha_{xz} \\ \alpha_{yx} & 1+\alpha_{yy} & \alpha_{yx} \\ \alpha_{yz} & \alpha_{zy} & 1+\alpha_{zz} \end{bmatrix} \begin{bmatrix} a_1 \\ a_2 \\ a_3 \end{bmatrix} = \begin{bmatrix} (1+\alpha_{xx})a_1 + \alpha_{xy}a_2 + \alpha_{xz}a_3 \\ \alpha_{yx}a_1 + (1+\alpha_{yy})a_2 + \alpha_{yx}a_3 \\ \alpha_{yz}a_1 + \alpha_{zy}a_2 + (1+\alpha_{zz})a_3 \end{bmatrix} = \begin{bmatrix} a_1' \\ a_2' \\ a_3' \end{bmatrix}$$

Now it is clear why the diagonal terms in the stress tensor e are added to 1. In that way the distorted lattice vectors become the primitive lattice vectors when the distortion parameter is set to zero.

Hooke's law is rewritten in terms of the stress tensor e_{ij} where the subscripts i and j can be x,y,z.

$$\sigma_{lm} = C_{lmij} e_{ij} \tag{4}$$

As the strain tensor is symmetric, there are six independent components, namely e_{xx}, e_{yy}, e_{zz}, e_{xy}, e_{xz} and e_{yz}. Each of them is multiplied with the elastic constant C from equation 4, thus C becomes a 6x6 tensor.

$$\begin{bmatrix} C_{11} & C_{12} & C_{13} & C_{14} & C_{15} & C_{16} \\ C_{21} & C_{22} & C_{23} & C_{24} & C_{25} & C_{26} \\ C_{31} & C_{32} & C_{33} & C_{34} & C_{35} & C_{36} \\ C_{41} & C_{42} & C_{43} & C_{44} & C_{45} & C_{46} \\ C_{51} & C_{52} & C_{53} & C_{54} & C_{55} & C_{56} \\ C_{61} & C_{62} & C_{63} & C_{64} & C_{65} & C_{66} \end{bmatrix} \begin{bmatrix} e_{xx} \\ e_{yy} \\ e_{zz} \\ e_{yz} \\ e_{zx} \\ e_{xy} \end{bmatrix} = \begin{bmatrix} \sigma_{xx} \\ \sigma_{yy} \\ \sigma_{zz} \\ \sigma_{yz} \\ \sigma_{zx} \\ \sigma_{xy} \end{bmatrix}$$

The elastic tensor can be reduced however to less elements depending on the symmetry of the crystal. This will be done in the next two sections 1.3.1 and 1.3.2 where the elastic constants for diamond and graphite are calculated.

From equation 4, it is obvious that C_{lmij} is a fourth rank tensor with (3x3)(3x3)=81 elements (as l,m,i,j can be x,y,z). To arrange those fourth rank tensor elements in a 6x6 matrix shown in 1.3, the Voigt notation is used where xx=1, yy=2, zz=3, yz=4, xz=5 and xy=6.

Now that the elastic tensor is defined, the method is presented with which its components are obtained. The elastic energy density U of a deformed crystal can be expressed in terms of the elastic tensor components $C_{\lambda\mu}$ where the λ and μ labels run from 1 to 6, according to the Voigt notation 1=xx, 2=yy, 3=zz, 4=yz, 5=xz and 6=xy.

$$U = \frac{1}{2} \sum_{\lambda=1}^{6} \sum_{\mu=1}^{6} C_{\lambda\mu} e_\lambda e_\mu \tag{5}$$

To extract the elastic constants $C_{\lambda\mu}$, the second order derivative of the energy density U with respect to the strain components e_λ and e_μ have to be calculated. The energy density U is just the total energy per atom divided by the volume per atom.

$$C_{\lambda\mu} = \frac{2}{V}\frac{\partial^2 E}{\partial e_\lambda \partial e_\mu} \tag{6}$$

The strain tensor components are a function of the lattice distortion parameter α, so it is reasonable to calculate the total energy per atom as a function of α. Once the total energy per atom is calculated as a function of the lattice distortion parameter α, one can apply a parabolic fit to the curve. The factor by which the crystal is stretched or compressed represents the second order derivative of the energy according to the Taylor expansion of the energy around the minimum which is at α=0.

$$E(\alpha) = E(0) + \frac{\partial E}{\partial \alpha}\alpha + \frac{\partial^2 E}{\partial \alpha^2}\alpha^2 \tag{7}$$

The second term in the expansion is zero as there is no force on any atom in equilibrium. So by fitting a parabola to the calculated energies, one finds the second order derivative of the energy with respect to the lattice distortion parameter α.

In the next two subsections the elastic constants of graphite in the AB Bernal stacking and diamond are calculated with the suggested method.

1.3.1 Graphite

In general, the elastic tensor has 6x6=36 components. Considering the symmetry of the crystal and of the strain tensor, this number can be reduced dramatically. The strain tensor is symmetric meaning that e_{ij}=e_{ji}, so C_{lmij}=C_{mlij}=C_{lmji}=C_{ijlm}. Only 21 components are left after that consideration.

Specifying to the symmetry of graphite, even more components can be neglected. Graphite has a hexagonal symmetry which means that by a $2\pi/6$ rotation around the z-axis, one can build the hexagon. After six rotations, one comes back to the starting point. This will happen equally, after rotation forward by a certain angle and then again backward by the same angle. Only those elastic tensor components will survive that are unchanged by any transformation, those are all which contain an equal amount of rotations in one plane direction and then in another like xxyy=12, transformations in only one plane direction like xxxx=11 (or yyyy=22 which is also in the rotation plane), rotations around the z-axis like zzzz=33, and rotations around the z-axis combined with rotations around x (or y) like xxzz=13 and xzxz=55.

There are thus five independent elastic constants, namely C_{11},C_{33},C_{55},C_{12} and C_{13}, all others are linear combinations of those.

To find the elastic constant C_{11}, the total energy per atom has to be calculated as a function of the lattice distortion parameter α where all elements in the strain matrix are set to zero except for e_{xx}=1+α.

$$\begin{bmatrix} 1+\alpha_{xx} & 0 & 0 \\ 0 & 1 & 0 \\ 0 & 0 & 1 \end{bmatrix} \begin{bmatrix} a_1 \\ a_2 \\ a_3 \end{bmatrix} = \begin{bmatrix} (1+\alpha_{xx})a_1 \\ a_2 \\ a_3 \end{bmatrix} = \begin{bmatrix} a_1' \\ a_2' \\ a_3' \end{bmatrix}$$

To find all other independent elastic constants, one can calculate them directly by putting all strain components to zero except for the strain components e_λ and e_μ that we want to consider.

To obtain the elastic constants, the volume per atom is important. In fig.26, a piece of graphene sheet is divided in areas which represent the area per atom.

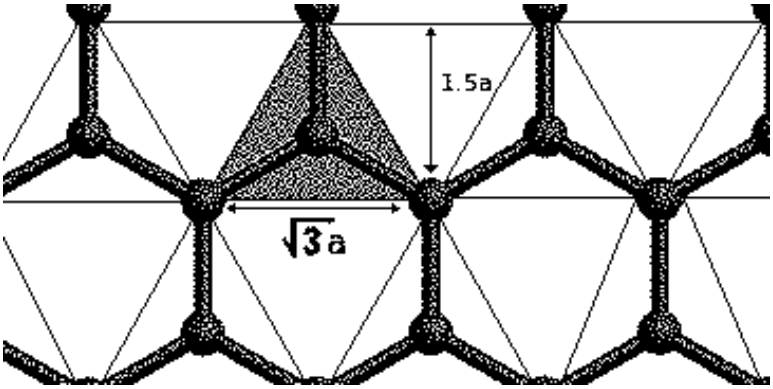

Figure 26: The area per atom is indicated by shaded triangle.

The area per atom is thus given by

$$\frac{1}{2}\sqrt{3} \cdot 1.5 \cdot (1.42)^2 = 2.62 \text{ Å}^2 \tag{8}$$

To obtain the volume per atom, one has to multiply the area per atom by the optimal interlayer distance which is 3.34 Å. The volume per atom in graphite is 8.75 Å^3.

1.3.2 Diamond

Diamond has a cubic symmetry. A rotation of $\pi/2$ around any of the three axes x, y and z enables the construction of the cubic cell. After four rotations or a rotation for- and backwards by the same angle, one comes back to the starting point. The independent elastic constants for a crystal with cubic symmetry are those that are not affected by any transformation.

For diamond, those independent elastic constants are C_{11},C_{12} and C_{44}. Again the total energy per atom is calculated as a function of α where the strain tensor is adjusted for every of those three cases.

The volume per atom is just the volume of the cubic cell that is spanned by the three lattice vectors introduced in section 1.2.5. The length for all three lattice vectors is 1.778 Å, so the volume per atom in diamond is (1.778 Å)^3=5.62 Å^3.

1.3.3 Results and discussion of elastic constants

In fig.27 the total energy per atom of graphite as a function of the lattice distortion parameter α for e_{xx} $\neq$0 and is shown together with a parabolic fit. The quadratic coefficient of the parabola is 28.825 eV and is equivalent to the second order derivative of the total energy per atom with respect to α.

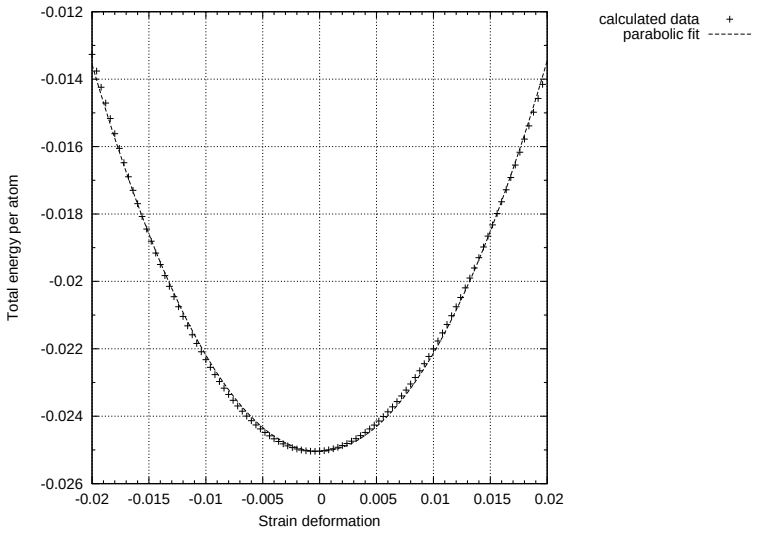

Figure 27: The total energy per atom (in eV) in graphite as a function of the lattice distortion parameter α (dimensionless) for strain component e_{xx}. The calculated data is fit by the parabola E(α)=-0.025+28.825α^2.

Filling all those values into formula 9, the following value is found for the elastic constant C_{11}.

$$C_{11} = \frac{2}{V}\frac{\partial^2 E}{\partial \alpha^2} = \frac{2}{8.75\ \text{Å}^3} 28.825\ \text{eV} = 6.588\,\frac{\text{eV}}{\text{Å}^3} \tag{9}$$

In fig.28 the total energy per atom of graphite as a function of the lattice distortion parameter α for e_{zz} $\neq$0 and the parabolic fit are shown. The quadratic coefficient of the parabola is 0.811 eV.

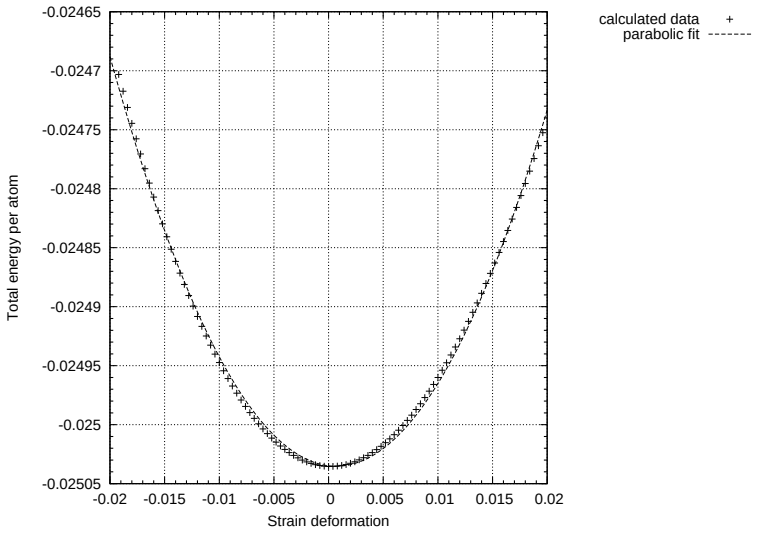

Figure 28: The total energy per atom (in eV) in graphite as a function of the lattice distortion parameter α (dimensionless) for strain component e_{zz}. The calculated data is fit by the parabola E(α)=-0.0011+0.811α^2.

Filling all values into formula 10, the elastic constant C_{33} is found to be

$$C_{33} = \frac{2}{V}\frac{\partial^2 E}{\partial \alpha^2} = \frac{2}{8.75\ \text{Å}^3} 0.811\ \text{eV} = 0.185\,\frac{\text{eV}}{\text{Å}^3}. \tag{10}$$

Now the elastic constant C_{11} for diamond is considered. In fig.29 the total energy per atom of graphite as a function of the lattice distortion parameter α for $e_{xx} \neq 0$ and the parabolic fit are shown. The quadratic coefficient of the parabola is 28.825 eV.

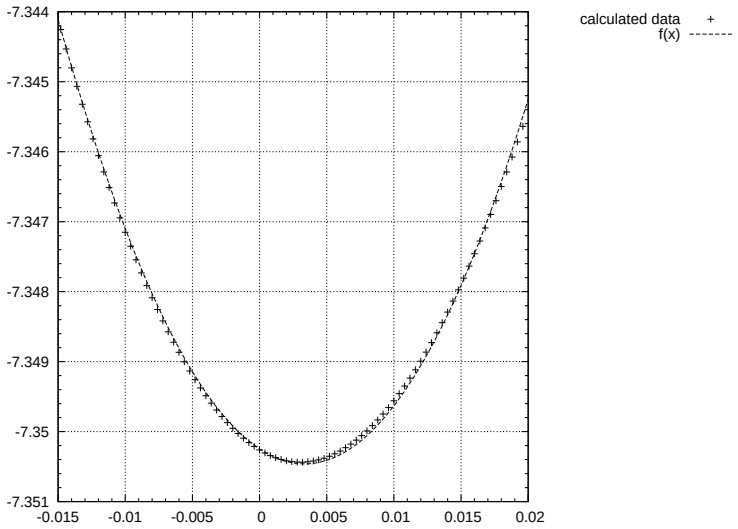

Figure 29: The total energy per atom (in eV) in diamond as a function of the lattice distortion parameter α (dimensionless) for strain component e_{xx}. The calculated data is fit by the function E(α)=-7.35+18.826α^2.

The elastic constant C_{11} is

$$C_{11} = \frac{2}{V}\frac{\partial^2 E}{\partial \alpha^2} = \frac{2}{5.62\ \mathring{A}^3} 18.826\ eV = 6.699 \frac{eV}{\mathring{A}^3}. \tag{11}$$

Elastic constants	Literature	
C_{11} (gr)	6.547	6.588
C_{33} (gr)	-	0.185
C_{11} (d)	6.718	6.699

Table 2: Elastic constants in eV/Å^3 for graphite (gr) and diamond (d) calculated with the method presented in subsection 1.3 and compared with values from the literature [7].

The calculated elastic constants for graphite and diamond are not in very good agreement with the values expected from the literature. They would be in much better agreement if the fits in figures 27, 28 and 29 where made in a smaller range around the minimum of the parabola. Indeed we see that the fits are not very good and that anharmonic terms already appear in the considered range giving rise to asymmetry around the minimum.

2 Procedure

The purpose of this master thesis is to push and slide different allotropes of carbon against each other and to understand the transformations caused by the process at the interface. To do this, we follow the trajectories of the atoms by means of a molecular dynamics simulation that we explain in the following.

To begin with, a starting sample has to be constructed. The carbon atoms can be arranged in different ways. In section 1.2 various types of carbon structures are presented. The following simulation is applied to each of the earlier mentioned carbon structures (graphite, diamond, clathrate and the low-energy structure) except for graphene. The focus lies on the sliding of bulk structures.

Two bulk structures are built that together have a total height of about 60 Å. Each bulk structure has a height of roughly 28 Å. The z-direction remains non-periodic.

Depending on whether a tip or a surface is pushed and slided against a surface, different approaches for building the in-plane dimensions are used.

When pushing and sliding two surfaces against each other, periodic boundary conditions are applied in the in-plane direction. That is why the length and width of the simulation box should be treated with caution. If both bulk structures are of the same lattice type, the width and length in the in-plane direction can be chosen arbitrarily. However, if the lattice types are not the same for both bulk structures, their lattice spacings do also differ. The width and length of the simulation box have to match both lattice spacings in such a way that the relative errors are small enough. A more detailed description for the choice of the in-plane dimensions for all simulations is presented in section 2.1.1.

When building the starting sample for the tip-surface simulation, other considerations are made. For more information, see the explanation in section 2.1.2.

In fig.30, the starting sample for pushing and sliding two (100)-surfaces against each other is shown. However, this scheme holds for any carbon structure that is pushed and slided.

In all cases, the two materials in the structure are separated by a distance of 2-4Å. Following reference [4], we place nine adatoms randomly in between. Those are atoms lying on a crystal surface, in order to prevent the welding or joining of surfaces. This phenomenon is called cold-welding as it can happen even without fusion or heating.

Then two layers are introduced at the top and at the bottom of the sample that both have a different function in the simulation. One layer is kept rigid, meaning that the atoms in this layer behave like one single entity, and moves with a constant velocity of v=30m/s. To the other one a Langevin thermostat is applied. They are quite thin compared to the total

height of the structure having a thickness of only a few atomic layers.

In order to push the structures together, a normal force is applied on the bottom rigid layer that is different for each simulation. The Langevin layers are thermalized using a Langevin thermostat at 300 K. The positions of the atoms in the remaining layers are updated using a constant NVE integration.

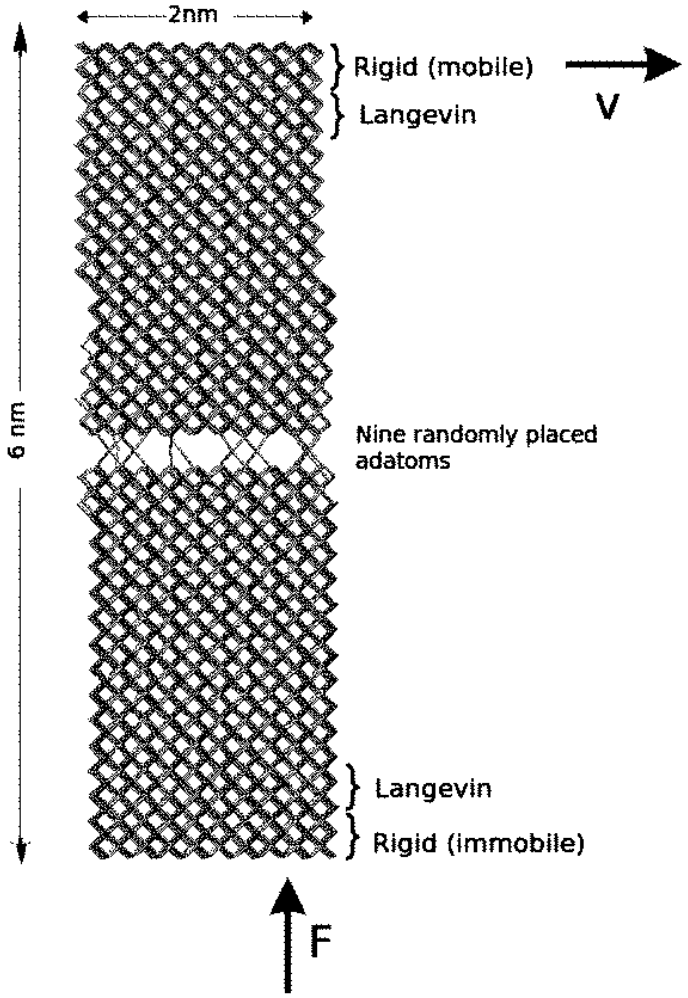

Figure 30: A visualization of the starting structure. Periodic boundary conditions are applied in the plane direction. The third dimension is non-periodic.

This simulation is carried out for two bulk carbon structures of the same kind ((100)-diamond on (100)-diamond, (111)-diamond on (111)-diamond, graphite on graphite, clathrate on clathrate, low-energy structure on low-

energy structure) and for two different kinds of bulk carbon-structures ((111)-diamond on graphite, (111)-diamond on clathrate, (111)-diamond on the low-energy structure, graphite on clathrate, graphite on the low-energy structure and clathrate on the low-energy structure).

The results are presented in section 5.

2.1 Generating samples

2.1.1 Surface on surface

Periodic boundary conditions are applied in the x- and y-direction. When building the bulk structures, the lattice spacings for two samples A and B with the simulation box dimensions a_x and b_x in x-direction and a_y and b_y in y-direction have to match. We require that the relative differences in x- and y-direction η_x and η_y are both less then 2%. This means that the strain in each structure can be accommodated elastically without causing drastic changes of the structures.

$$\eta_x = \frac{a_x - b_x}{a_x} \leq 2\% \text{ and } \eta_y = \frac{a_y - b_y}{a_y} \leq 2\% \tag{12}$$

Both materials A and B have characteristic lattice spacings x_A and x_B in x-direction and y_A and y_B in y-direction. They have to be repeated n_{ax} and n_{bx} in x-direction, and n_{ay} n_{by} in y-direction such that the simulation box dimensions $a_x = n_{ax} x_A$, $a_y = n_{ay} y_A$, $b_x = n_{bx} x_B$ and $b_y = n_{by} y_B$ lead to the desirable relative errors.

The following two tables show how often the lattice spacings have to be repeated in x- and y-direction to achieve relative errors less than 2%.

Samples	n_{ax}	n_{bx}	x_A in Å	x_B in Å	η_x in %
Diamond(A)-graphite(B)	12	7	2.51	4.26	0.996007
Clathrate(A)-diamond(B)	4	21	13.22745	2.51	0.377628
Low-energy structure(A)-diamond(B)	7	13	4.685	2.51	0.503117
Clathrate(A)-Graphite(B)	10	31	13.22745	4.26	0.162157
Low-energy structure(A)-graphite(B)	11	12	4.685	4.26	0.805272
Clathrate(A)-low-energy structure(B)	5	14	13.22745	4.685	0.827456
Graphite(A)-graphite (rotated by 30 °)(B)	7	12	4.26	2.46	1.028580

Table 3: Choices for n_{ax} and n_{bx} to achieve relative errors $\eta_x \leq 2\%$. Actually the maximum relative error for the indicated n_{ax} and n_{bx} is 1%.

Samples	n_{ay}	n_{by}	y_A in Å	y_B in Å	η_y in %
Diamond(A)-graphite(B)	7	10	3.55	2.46	1.006036
Clathrate(A)-diamond(B)	3	11	13.03115	3.55	0.111142
Low-energy structure(A)-diamond(B)	9	11	4.34409	3.55	0.119729
Clathrate(A)-Graphite(B)	4	21	13.03115	2.46	0.891325
Low-energy structure(A)-graphite(B)	4	7	4.34409	2.46	0.899836
Clathrate(A)-low-energy structure(B)	17	50	13.03115	4.34409	1.952355
Graphite(A)-graphite (rotated by 30 °)(B)	12	7	2.46	4.26	1.028580

Table 4: Choices for n_{ay} and n_{by} to achieve relative errors $\eta_y \leq 2\%$.

2.1.2 Tip on surface

We have also considered the sliding of a finite tip on a surface.

The carbon atoms contained in the simulation box shown in fig.31 are arranged according to the pattern of a diamond cubic structure. There are 30458 atoms present out of which 4058 atoms form the tip.

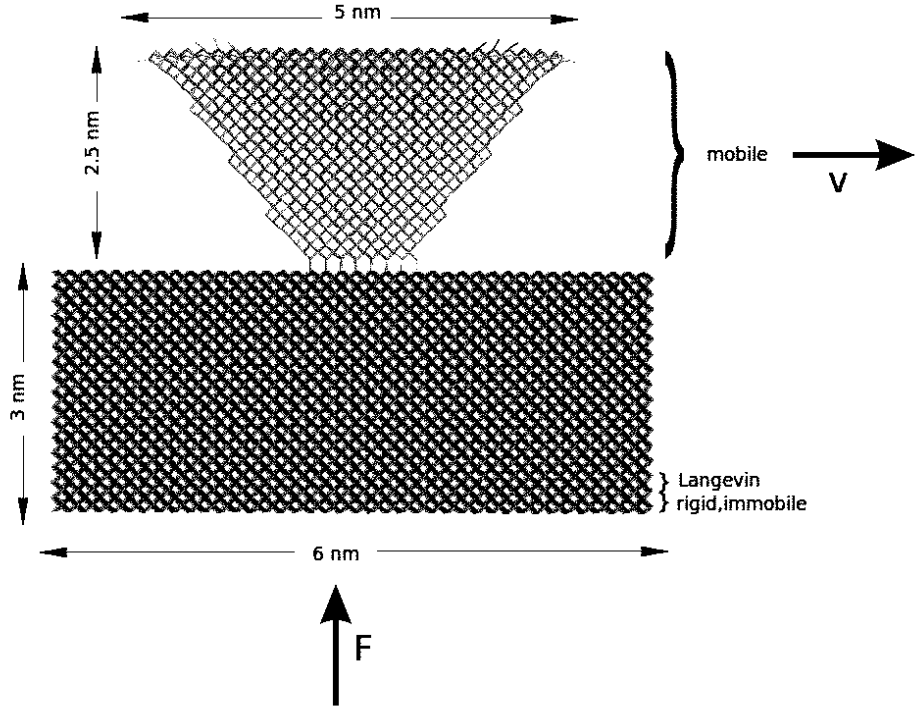

Figure 31: A visualization of the starting structure. Periodic boundary conditions are applied in the x- and y-direction.

In this case, it is not necessary to consider the match the lattice spacings of the structures in contact when applying periodic boundary conditions in the x- and y-direction. When the tip is moved and crosses the boundary, it will be mapped again to the other side of the boundary. One has to be only careful that the carbon atoms at both sides of the boundary do not interact through the LCBOB potential which has a maximum cut-off of 6 Å(see fig.5). When the tip crosses the boundary, its last carbon atom should be at least 12 Å away from its first carbon atom entering from the other side of the boundary.

3 Methods

3.1 Molecular dynamics

The samples that are studied in experiments are usually macroscopic, thus visible with the naked eye. They consist of a very large number of atoms in many different states. To study physical properties of the system, we need observables. The measurement and calculation of those observables is challenging because all atoms in all states contribute to the physical property of interest. To simplify this problem, averages are used.

In experiments, the average of a physical property is measured as an average over a large particle number and usually as an average over time.

In numerical experiments, different approaches are possible. One of these is the Monte Carlo method. It is based on classical statistical physics where observables are predicted statistically by ensemble averages in the canonical ensemble, namely with constant volume, number of particles and temperature. The ensemble average of some observable $<A>_{ensemble}$ is expressed as an integral over the whole phase space.

$$< A>_{ensemble} = \int\int dp_N dq_N A(p_N, q_N)\rho(p_N, q_N) \tag{13}$$

The probability density $\rho(\mathrm{p}_N,\mathrm{q}_N)$ in the NVT ensemble is given by the Boltzmann distribution

$$\rho = \frac{1}{Q} e^{\frac{H(p_N,q_N)}{k_B T}} \tag{14}$$

and Q stands for the partition function.

$$Q = \frac{1}{N! h^{3N}} \int\int dp_N dq_N e^{\frac{H(p_N,q_N)}{k_B T}} \tag{15}$$

To find thus $<A>_{ensemble}$, we need to integrate over all possible states of $\mathrm{A}(\mathrm{p}^N,\mathrm{q}^N)$, an almost impossible task for interacting particles.

The Monte Carlo method gives an alternative way to calculate $<A>_{ensemble}$ by generating many different states with an appropriate Boltzmann distribution. Basically, an ensemble average describes all possible states of the system at equilibrium without giving any information on temporal behaviour.

Another approach are molecular dynamics simulations where the averages of a given quantity at equilibrium $<A>_{time}$ are calculated as time averages over a long enough length of time τ.

$$< A>_{time} = \lim_{\tau\to\infty} \frac{1}{\tau} \int_{t=0}^{\tau} dt A(p_N(t), q_N(t)) \tag{16}$$

The integral can be approximated by a sum. In this case, the continuous integration variable time t becomes a discrete index. That is why the maximum number of timesteps T is used in the approximation, instead of the period of time τ.

$$< A>_{time} \approx \frac{1}{T} \sum_{t=1}^{T} A(p_N(t), q_N(t)) \tag{17}$$

The ergodic hypothesis states that $<A>_{time}$ is equal to $<A>_{ensemble}$ implying that the system will visit all possible microstates in its trajectory. By molecular dynamics one can not only calculate static equilibrium properties but also follow the system in time and get information on the dynamics.

The basis of molecular dynamics simulations is built on classical mechanics. The second law of Newton states that the force $\vec{F_i}$=$m_i\vec{a}_i$, where m is the mass and $\vec{a}_i$ the acceleration of a particle i in all Cartesian directions. Once the force is known, one can determine the acceleration of all particles in the system, and thus all velocities and positions.

$$F_{ix} = m_i a_{ix} = m_i \frac{\partial v_{ix}}{\partial t} = m_i \frac{\partial^2 x_i}{\partial t^2} \tag{18}$$

For conservative forces,

$$\vec{F_i} = -\vec{\nabla} V_i(\vec{q_i}) \tag{19}$$

where $\mathrm{V}_i(\vec{q_i})$ is a potential depending only on the coordinates.

If we connect formula (18) with formula (19), the following relation is found.

$$a_{ix} = \frac{\partial^2 x_i}{\partial t^2} = -\frac{1}{m_i} \frac{\partial V_i(x_i)}{\partial x_i} \tag{20}$$

The position of each particle is thus given by $\vec{q_i} = \frac{1}{2}\vec{a}_i t^2 + \vec{v}_i t + \vec{q}_{i0}$, where $\vec{q}_{i0}$ is the initial position of the atom in the simulation. To calculate the evolution in time of the particle's positions $\vec{q_i}$, also called trajectory, one needs the initial positions of the atoms $\vec{q}_{i0}$ and an initial distribution of

the accelerations $\vec{a}_i$ and the velocities $\vec{v}_i$. The initial velocities can be chosen from a Maxwell-Boltzmann or a Gaussian distribution. One can calculate the position and velocity of each particle for every timestep by means of a numerical integration method. There are many algorithms that can do that. Here, the velocity Verlet integration algorithm is presented based on a discretization of Newton's equations of motion for a uniformly accelerated motion[19].

Expressing each particle's positions after a time interval δt by

$$q_i(t+\delta t) = q(t) + \frac{dq_i}{dt}\delta t + \frac{1}{2}\frac{d^2q_i}{dt^2}\delta t^2 \tag{21}$$

as well as before the time interval δt

$$q_i(t-\delta t) = q(t) - \frac{dq_i}{dt}\delta t + \frac{1}{2}\frac{d^2q_i}{dt^2}\delta t^2 \tag{22}$$

and adding both equations (21) and (22) up, will lead us to the following expression.

$$q_i(t+\delta t) = q_i(t) - q_i(t-\delta t) + a_i(t)\delta t^2 \tag{23}$$

Equation 23 has the disadvantage that the velocities disappear which can be useful for the calculation of the kinetic energy.

The velocity Verlet algorithm updates positions and velocities in two phases. First, we advance the positions by a time step δt and the velocities by δt/2 using the forces calculated at time t from the q_i(t).

$$q_i(t+\delta t) = q_i(t) + v_i(t)\delta t + \frac{1}{2}a_i(t)\delta t^2 \tag{24}$$

$$v_i(t+\frac{\delta t}{2}) = v_i(t) + a(t)\frac{1}{2}\delta t \tag{25}$$

Then with the new positions $q_i(t+\delta t)$ we calculate the forces at t+δt and reduce the velocities from t+δt/2 to t+δt using these forces.

$$v_i(t+\delta t) = v_i(t+\frac{\delta t}{2}) + a(t+\delta t)\frac{1}{2}\delta t \tag{26}$$

The acceleration depends on the potential and can be obtained by formula 20. The potential used in the simulation is discussed in the following subsection. So once you have an initial distribution of the positions and a potential, you can follow the trajectory of each atom.

It is important to choose an appropriate timestep for the simulation. Picking a too small time step will waste computer time. If the timestep is too large, the dynamics become unstable and the energy will not be conserved and increase.

3.2 Empirical potential LCBOP

Carbon can take on different structures with characteristic thermodynamic and structural properties. To describe these features of carbon in molecular dynamics simulations, bond order potentials (BOP) are used.

There are many well-known BOP's like the Tersoff or Brenner potential which describe different coordination states of atoms well. They are also called reactive potentials as they account well for chemical reactions. The idea behind BOP's is that the strength of chemical bonds depends on the bonding environment of the atoms, or with other words, their number of nearest neighbours, their bond length and even bond angle.

If the number of nearest neighbours for an atom is for instance high, the chemical bonds are weak as the electrons have to be distributed among many neighbours. The chemical bonds are also weak for too high or too small bond lengths because each pair of atoms has its characteristic bond length for which the total energy per atom is in its minimum.

BOP's are actually short-range potentials that decrease with distance with a certain cut-off distance at which the atoms do not form chemical bonds anymore. The short-range potential V_{SR} between two atoms at distance r_{ij} is presented in formula 27 where V_R describes the core repulsion between the pair of atoms, V_A their attraction and B_{ij} the bond-order, a many-body parameter that depends on the bonding-environment of the atoms.

$$V_{ij}^{SR} = V_R(r_{ij}) - B_{ij}V_A(r_{ij}) \tag{27}$$

To be more precise, the repulsive and attractive potentials are defined as V_R=Aexp(-θr) and V_A=-Bexp(-λr) where A, λ and θ are parameters that are fitted to experimental data, and B is a complex function of the interatomic distances, bond angles and coordinations. That is why BOP's are called empirical (derived from the Greek word εμπειρία ,"experience, practical knowledge").

This short range potential is not sufficient enough to describe the crystalline phases of carbon and its different coordination states. For instance graphite has strong covalent bonds within the layers and a weak van der Waals attraction between them[10].

To model this long-range interaction in carbon, J.H. Los and A. Fasolino proposed the "Long range Carbon Bond Order Potential" or LCBOP in short form.

An additional long-range potential V^{LR} is introduced that implements a force between all atoms beyond the first nearest neighbours creating an additional shallow minimum at the interlayer distances of graphite. Formula 28 represents the binding energy E_b that is a result of the short- and long-range interactions of all pairs of atoms. The function f_{ij} is a smooth cut-off

function and S_{ij} is a switching function excluding interactions with first nearest neighbours.

$$E_b = \frac{1}{2}\sum_{i,j}^{N}(f_{ij}V_{ij}^{SR} + S_{ij}V_{ij}^{LR}) \tag{28}$$

To achieve correct equilibrium lattice parameters for the different allotropes of carbon (e.g. 1.54 Å for diamond and 1.42 Å for graphite), the additional long-range repulsion by the second nearest neighbours is corrected by a stronger short range attraction between the first nearest neighbours.

It should be stressed that LCBOP is not built by adding a long-range potential to an established short range potential. This sort of empirical potentials exist and are detrimental to the accuracy. They demand a special approach such that the short-range and long-range potentials do not create unphysical barriers for transitions like graphite to diamond. In LCBOP, this problem is tackled by a suitable parameterization of the short-range part[7].

3.3 Conjugate gradient algorithm

The carbon atoms in the proposed starting samples in section 2 are placed on different crystal lattices (graphite, diamond, clathrate etc.) at certain positions that are repeated periodically in x- and y-direction. The atoms interact through the long-range bond order potential for carbon LCBOP (see section 3.2) which depends on the positions of the atoms.

The potential energy is a function of all possible atomic positions. It is a function of 3N-6 coordinates, where N is the number of atoms in the three-dimensional system. The rotation and translation of the system as a whole is not considered, that is why six coordinates are removed. For a different set of positions, the potential energy can change.

The initial positions given to the atoms might not correspond to a minimum value of the potential energy. It is important to note that for more complex systems, their atomic positions are not consistent with the global minimum of the potential energy, but with one of the plenty of local minima. These local minima are also called metastable. The system might sit in such a state for a while or even forever. The quest for the global minimum is discussed in section 3.4.

Suppose the atomic positions at the beginning do not correspond to a minimum of the potential energy. It means that the system is not in equilibrium and thus not stable. To find the atomic positions for which the system is stable, the following considerations are made.

The atomic starting positions are described by the multidimensional point $\mathbf{P}$. Consequently, f($\mathbf{P}$) is the value of the potential energy at that point and ∇f($\mathbf{P}$) is the first partial derivative of the function at that point.

The function f is approximated near point **P** by a Taylor approximation presented in formula 29.

$$f(\boldsymbol{x}) = f(\boldsymbol{P}) + \sum_i \frac{\partial f}{\partial x_i} x_i + \frac{1}{2} \sum_{i,j} \frac{\partial^2 f}{\partial x_i \partial x_j} x_i x_j + ... = c - \boldsymbol{b} \cdot \boldsymbol{x} + \frac{1}{2} \cdot \boldsymbol{x} \cdot \boldsymbol{A} \cdot \boldsymbol{x} \quad (29)$$

Changing any of the parameters c=f(**P**), **b**=-$\nabla f|_{\boldsymbol{P}}$ and $[\mathbf{A}]_{ij}=\frac{\partial^2 f}{\partial x_i \partial x_j}|_{\boldsymbol{P}}$ can lead us to a minimum of f where the its gradient ∇f is zero. Differentiating formula 29 with respect to x, leads to the following formula.

$$\nabla f = \boldsymbol{A} \cdot x - \boldsymbol{b} \quad (30)$$

The potential energy f is in one of its minima for **A** · **x**=**b**. One idea to tackle this aspect is by starting out at some $\mathbf{P}_0$ and to move in small steps i along the line of the downhill gradient -∇ f($\mathbf{P}_i$). This method is called steepest descent method and is not very efficient. It might lead to any valley, even if the minimum does not have a perfect quadratic form. A much better method is the conjugate gradient algorithm. The name will become evident in the following.

The change of the gradient $\delta(\nabla \mathrm{f})=\mathbf{A}\cdot(\delta \boldsymbol{x})=\mathbf{A}\cdot\mathbf{v}$ is followed along some direction **v**. Suppose now, that we want to move along another direction **u**. Equation 31 needs to be satisfied or otherwise the minimization cannot be performed.

$$\boldsymbol{u}^T \cdot \delta(\nabla f) = \boldsymbol{u}^T \cdot \boldsymbol{A} \cdot \boldsymbol{v} = 0 \quad (31)$$

The matrix **A** is symmetric and positive definite so it is equal to its transpose $\mathbf{A}^T$. Two vectors **v** and **u** are defined as conjugated, if $\boldsymbol{u}^T \cdot \boldsymbol{A} \cdot \boldsymbol{v} = 0$. This is only the case if these two vectors are perpendicular to each other, that is to say when their inner product $< \boldsymbol{u}, \boldsymbol{v} >= 0$.

$$\boldsymbol{u}^T \cdot \boldsymbol{A} \cdot \boldsymbol{v} =< \boldsymbol{u}, \boldsymbol{A}\boldsymbol{v} >=< \boldsymbol{u}, \boldsymbol{A}^T\boldsymbol{v} >=< \boldsymbol{A}\boldsymbol{u}, \boldsymbol{v} >=< \boldsymbol{u}, \boldsymbol{v} > \boldsymbol{A} = 0 \quad (32)$$

Performing line minimizations along a set of conjugate vectors will lead to a minimum with a quadratic form (see fig 32)[12].

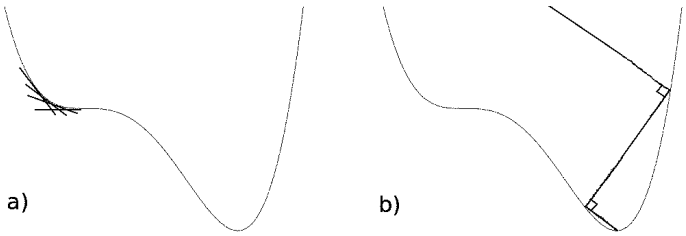

Figure 32: a)Two-dimensional schematic illustration of the steepest gradient method leading to a narrow valley in comparison to b) where the conjugated gradient algorithm quickly leads to a minimum with a quadratic form.

3.4 Simulated annealing

In the previous section 3.3 it is mentioned that the atomic positions of most systems in equilibrium do not correspond to the global minimum of the potential energy, but to one of its local minima. By means of the earlier explained conjugate gradient algorithm it is possible to find a minimum starting from some point close to it. It is not possible to overcome energy barriers in order to find lower minima or even the global one.

There are many global minimization algorithms. The quest for the global minimum has become a research field on its own. The method to find global minima for our carbon structures that is used here is called simulated annealing.

To move to a higher point on the potential energy, the energy of the system needs to be increased. The next step is to keep the energy constant for a while in order to move in plane to another point. At the end the energy needs to be to decreased in order to reach a lower, and hopefully the lowest one, on the potential energy. The energy is increased, equilibrated and decreased by tuning the temperature over a certain time interval.

To tune the temperature of our systems a technique called Nosé-Hoover thermostat is used. To ensure fluctuations of the total energy, an external heat bath is added to the system. An additional variable $\bar{s}$ is introduced in the Hamiltonian to change the kinetic energy in such a way that the desired temperature can be reached. The velocities are changed accordingly.

The variable $\bar{s}$ is a time scaling parameter and connected to another parameter Q and a velocity $\dot{\bar{s}}$. The time scale in the extended system becomes $d\bar{t}$sdt. The atomic coordinates remain the same ($\bar{\mathbf{r}}$=r) and their velocities become $\dot{\bar{\mathbf{r}}} = \dot{\mathbf{r}}/\bar{s}$.

The extended system is described by the following Lagrangian.

$$\mathcal{L} = \sum_i \frac{m}{2}\bar{s}^2\dot{\bar{\mathbf{r}}}_i - U(\bar{\mathbf{r}}) + \frac{1}{2}Q\dot{\bar{s}} - Nk_BT_0 \ln \bar{s} \tag{33}$$

The first two terms are simply the kinetic and potential energy of the real system and the last ones are the kinetic and potential energy of the additional system where N is the number of atoms and k_B the Boltzmann constant.

This Lagrangian leads to the Nosé equations of motion.

$$\ddot{\bar{\mathbf{r}}}_i = \frac{\bar{F}_i}{m_i \bar{s}^2} - \frac{2\dot{\bar{s}}\dot{\bar{\mathbf{r}}}_i}{\bar{s}} \tag{34}$$

$$\ddot{\bar{s}} = \frac{1}{Q\bar{s}} \left(\sum_i m_i \bar{s}^s \dot{\bar{\mathbf{r}}}_i^2 - N k_B T_0 \right) \tag{35}$$

The parameter Q determines how fast the temperature fluctuations are applied on the system. So if the desired temperature is high, the velocity and the kinetic energy of the particles are high and vice versa. The kinetic energy of the particles depends on the temperature. So if the temperature is increased, the atoms gain energy to overcome the energy barrier. By keeping the temperature constant, the atoms move on a certain constant energy level. When the temperature is cooled down slowly the atoms lose energy[13].

Integrating the equations of motion is done by means of the Verlet algorithm that is described earlier (see section 3.1).

3.5 Langevin thermostat

Langevin dissipation is a way to describe the irreversible dissipation of energy into heat that is needed in order to keep the temperature constant. The forces are modified according to the Langevin equation that contains the forces between the particles, a random force, that fluctuates over time but is zero on average, and a damping force.

Basically, the Langevin thermostat is an application of the fluctuation-dissipation theorem that states that the reaction of a system on a small external disturbance is the same as its reaction on a fluctuation.

In the simulation explained in section 2, a Langevin thermostat is applied on the atoms above and beneath the bottom and top rigid layer. The temperature is kept at 300K. It is a challenge to find the damping parameter which damps the change in temperature after a certain number of timesteps. There is no straightforward method to find the damping parameter as it depends strongly on the system.

The damping parameter is given in time units, but usually it is given in inverse time units (F=γmv, so γ has units 1/s). The damping coefficient may be also called viscous damping coefficient as it provides damping linear with the velocity. So if the viscosity is high, the damping force is also high, which means that the structure is not likely to behave as a fluid. And as

the damping coefficient in the Langevin command is given in units time it is inversely proportional to the viscosity coefficient which is given in kg/s. So for a high viscous fluid, a small damping time should be chosen.

To find the damping coefficient, a molecular dynamics simulation without any thermostat is performed for two (111)-diamond surfaces that are pushed together and slides. The number of timesteps as a function of the temperature is shown. The results are presented in fig.33.

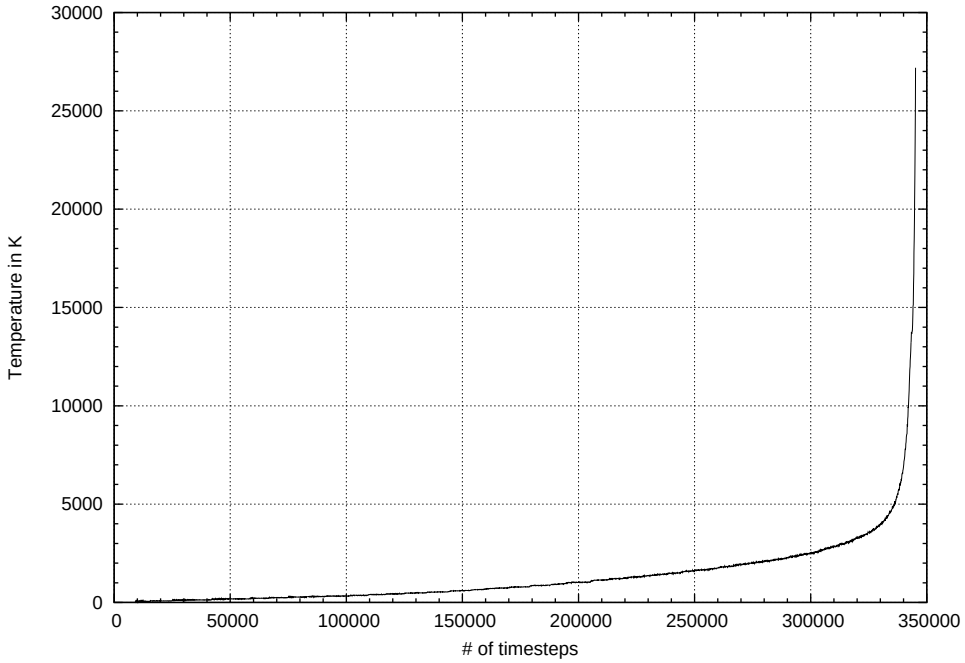

Figure 33: The temperature as a function of the number of timesteps without any thermostat.

As we can see in fig.33, the temperature blows up after roughly 350.000 timesteps. The timestep of the simulation is 1fs, thus the timespan of 350.000 timesteps is 350 ps. The damping parameter should be thus 350. However already much earlier the system reaches the temperature we should like to have. That is why this damping parameter does not work for our simulations. A smaller one is needed. After many attempts, the best choice turns out to be $6 \cdot 10^{-4}$ ps, or 0.6 fs.

3.5.1 LAMMPS

The molecular dynamics simulations are performed by means of the classical molecular dynamics code "Large-scale Atomic/Molecular Massively Parallel Simulator" or LAMMPS. It is an open source code which means that it can be modified, extended and used for free. This permission is guaranteed by

the GNU General public license.

Users may carry out simulations on soft and solid-state materials and investigate effects on the atomic scale. LAMMPS provides a broad range of potentials to model pairwise interactions between all different kinds of atoms. The potential used in this master thesis is LCBOP and is discussed in section 3.2.

What makes LAMMPS so special is its ability to perform several operations at the same time. The code is divided into smaller pieces each of them run on different CPU's ("Central processing units") or cores. It might sound trivial but achieving this without having the subparts of the code interfering with each other is quite challenging. The advantage of parallel processing is that the code as a whole runs faster.

LAMMPS is developed and maintained by the Sandia National Laboratories which belongs to the United States Department of Energy. It is a research and development laboratory in the United States that focusses on national security and nuclear science[11].

4 Analysis methods

4.1 Radial distribution function

To extract information on how the atoms are organized, the radial distribution function is used. It is a measure of how many atoms are found at a certain distance from another atom.

Suppose there are N particles in a volume V at some temperature T. They can exist in different configurations that are defined by the classical configurational distribution $\mathrm{P}^{\frac{n}{N}}(\mathbf{r}_1,...,\mathbf{r}_N)$ which expresses the probability for finding all possible configurations of n out of N particles at positions $\mathbf{r}_1,...,\mathbf{r}_N$ where $\mathrm{U}_N(\mathbf{r}_1,...,\mathbf{r}_N)=\mathrm{U}_N$ is the interaction potential between all particles.

$$P^{\frac{n}{N}}(\boldsymbol{r_1},...,\boldsymbol{r_N}) = \int d\boldsymbol{r_1} \int d\boldsymbol{r_2}... \int d\boldsymbol{r_N} e^{-\frac{U_N}{k_B T}} \tag{36}$$

By means of the configurational distribution $\mathrm{P}^{\frac{n}{N}}$, the number density function $\boldsymbol{\rho}^{\frac{n}{N}}$ for finding a particle while the n out of N positions $\mathbf{r}_1,...,\mathbf{r}_n$ are fixed, is expressed in the following equation.

$$\rho^{\frac{n}{N}}(\boldsymbol{r_1},..,\boldsymbol{r_n}) = \frac{N!}{(N-n)!} \frac{\int d\boldsymbol{r_{n+1}}... \int d\boldsymbol{r_N} e^{-\frac{U_N}{k_B T}}}{P^{\frac{n}{N}}} \tag{37}$$

For an isotropic fluid where only one position, for instance $\mathbf{r}_1$, is fixed the number density is simply $\boldsymbol{\rho}^{\frac{1}{N}}=\rho=\mathrm{N/V}$.

In an ideal gas, particles do not interact with each other. The Hamiltonian of the whole particle system can be split in single Hamiltonians for each

particle. Their positions are therefore independent from each other. The particles are uncorrelated. That is why he probability for finding a particle at $\mathbf{r}_1$ and another at $\mathbf{r}_2$ can be written as $\mathrm{P}^{\frac{2}{N}}(\mathbf{r}_1,\mathbf{r}_2) = \mathrm{P}^{\frac{1}{N}}(\mathbf{r}_1)\mathrm{P}^{\frac{1}{N}}(\mathbf{r}_2)$.

The number density for an ideal gas for finding one particle at $\mathbf{r}_1$ and any other at $\mathbf{r}_2$ is

$$\rho^{\frac{2}{N}}(\boldsymbol{r_1}, \boldsymbol{r_2}) = \frac{N(N-1)}{V^2} = \rho^2(1 - \frac{1}{N}) \approx \rho^2 \tag{38}$$

The approximation in the last step of formula 38 is applied under the assumption that the number of atoms is very large.

The atoms are modelled as spherically symmetric particles that are distributed homogeneous over the whole space (see fig.34).

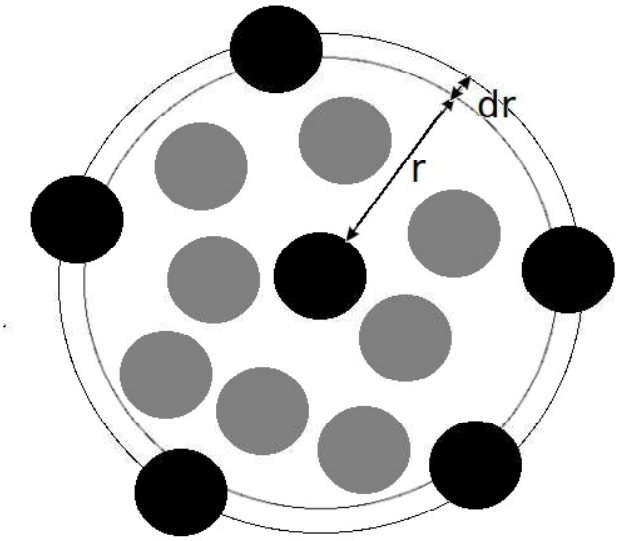

Figure 34: The radial distribution function is a measure of how the density of atoms varies for different distances from a reference particle (black sphere in the middle).

The number density of the atoms is calculated as a function of their distance to the reference atom and normalized by the ideal gas number density function. With other words, the density at different points in space is divided by the density of the whole system.

$$g(\boldsymbol{r_1}, \boldsymbol{r_2}) = \frac{\rho^{\frac{2}{N}}(\boldsymbol{r_1}, \boldsymbol{r_2})}{\rho^2} \tag{39}$$

Under the assumption that the atoms are spherical and part of an homogeneous substance, the normalized function $\mathrm{g}(\mathbf{r}_1,\mathbf{r}_2)$ depends only on the

magnitude of the difference between the two vectors $|\mathbf{r}_1 - \mathbf{r}_2|$=$r_{12}$. This new function g(r) is called radial distribution function[8].

To determine the radial distribution function, one has to calculate how many atoms are at a certain distance from the reference atom. Therefore, one needs all distances between all atom pairs. To determine the number of atoms at a certain distance, the δ-function is used that is zero everywhere except at the origin. So whenever the distance r_{ij} between the reference atom and another atom is equal to the binning distance r, the δ-function is equal to unity. It thus counts how many atoms are found at a certain distance from the reference atom. The radial distribution function is defined as follows where the angular brackets stand for the time average[9].

$$\frac{\rho^{\frac{2}{N}}(r)}{\rho} = \rho g(r) = \frac{1}{N}\langle \sum_{i=1}^{N} \sum_{j \neq i}^{N} \delta(r - r_{ij}) \rangle \tag{40}$$

4.2 Coordination number

Another way to analyze structures is to calculate the coordination number for each of their atoms. Each atom has one or more nearest neighbours. The coordination number reveals information on how many nearest neighbours an atom has. If an atom has one nearest neighbor, its coordination number is 1, if it has two, its coordination number is 2, and so on.

To calculate the coordination number for each atom in a structure with periodic boundary conditions in each cartesian direction, a program in C/C++ is developed which is attached to the appendix in section 7.1.

The only information the program needs, are the positions of the atoms at each timestep and the three lattice vectors $\mathbf{a}_1$, $\mathbf{a}_2$ and $\mathbf{a}_3$ defining the simulation box in which the atoms are arranged. Molecular dynamics simulations keep track of the trajectories and the positions ($\mathbf{x}_i$,$\mathbf{y}_i$,$\mathbf{z}_i$) of all N atoms (i=1,2,...,N) at each timestep.

Once this data is loaded, the mutual distances r_m(i,j) between all atom pairs (i,j) are obtained.

$$r_m(i,j) = \sqrt{(x_j - x_i)^2 + (y_j - y_i)^2 + (z_j - z_i)^2} \tag{41}$$

Usually r_m^2 is calculated to avoid the square root and to save computer time. The condition for bonding is $r_m^2 \leq (2.2\ \text{Å})^2$.

As periodic boundary conditions are applied, the distances from the atoms to the atoms across the boundaries become also crucial. Therefore, auxiliary atoms are introduced that are projected along the lattice vectors and their linear combinations.

In fig.35, the idea is explained by means of a two-dimensional box with two basis atoms in it. Within the box, the two atoms, depicted as black dots, are too far apart and would not be nearest neighbours. Taking the

projected, grey atoms into account, one sees that the two atoms are indeed nearest neighbours.

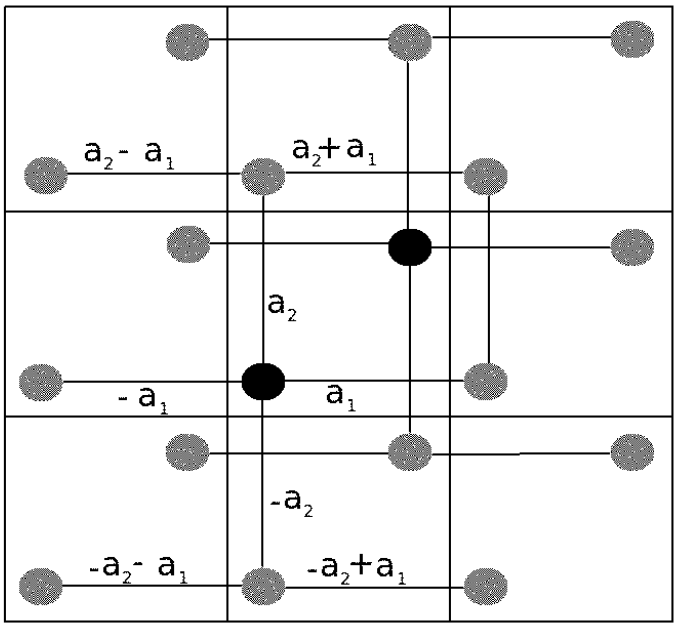

Figure 35: The black dots represent the original atoms in the box and the grey dots stand for the projected atoms.

Once the distances between all original atoms with each other and their projected atoms are known, the number of nearest neighbours can be calculated. Each pair of elements has a specific bond length up to which bonds are formed. For pairs of carbon atoms this distance has a maximum of 2.2 Å. All pairs of atoms that have distances not longer than this cutoff distance, are counted as nearest neighbours. As already mentioned, the condition for bonding is $r_m^2 \leq (2.2\ \text{Å})^2$. The output of the code presented in section 7.1 gives the number of nearest neighbours for each atom at each timestep.

4.3 Characterization of the temperature per layer via equipartition

The two bulk structures that are pushed together are divided into several layers. Each layer has a different environment in the simulation box and therefore experiences a different force from the others.

These forces acting on each atom in absence of external forces make it move with a certain velocity in the three-dimensional space. However, it is convenient to require to have no overall linear momentum in order to prevent the system from moving as a whole.

$$p(t=0) = \sum_{i=1}^{N} m_i v_i = 0 \tag{42}$$

During the dynamics, the velocities in all three spatial directions (v_{ix}, v_{iy} and v_{iz}) can be calculated for each atom. From those velocities, the kinetic energy per atom E_{Kin} can be calculated where m is the mass of one carbon atom.

$$E_{Kin} = \frac{1}{2} m (v_{ix}^2 + v_{iy}^2 + v_{iz}^2) \tag{43}$$

The equipartition theorem says that every component of the momentum or the position that appears quadratically in the total energy, has an average energy of $1/2 k_B T$, where k_B is the Boltzmann constant. In the presented case, there are three velocities that appear quadratically in the total energy per atom, thus the average kinetic energy per atom i equals $3/2 k_B T$.

$$\frac{1}{2} m (v_{ix}^2 + v_{iy}^2 + v_{iz}^2) = \frac{3}{2} k_B T \tag{44}$$

Using the above mentioned equation, it is possible to extract the T. It is just a rearrangement of variables and has no physical meaning. There is no temperature per atom and T becomes a measure of temperature only when averaging over many atoms.

The sample is now divided into layers with a certain thickness. Then, it is determined which atom belongs to which layer and the number of atoms N_{layer} per layer is calculated. To find the temperature per layer T_{layer} the sum over all T is taken and divided by the number of atoms in the layer N_{layer} .

$$T_{layer} = \frac{1}{N_{layer}} \sum_{i=1}^{N_{layer}} T_i = \frac{1}{N_{layer}} \sum_{i=1}^{N_{layer}} \frac{1}{3k_B} m (v_{ix}^2 + v_{iy}^2 + v_{iz}^2) \tag{45}$$

The temperature T_{layer} is calculated for all layers as a function of time.

5 Results and discussion

In the following, the results are presented and discussed for the simulation described in section 2. The construction of the simulation boxes for the samples in question is treated in section 2.1.

5.1 Tip on surface for (100)-diamond

First, the results are presented for the simulation of a tip slided on a surface. It is carried out for a (100)-diamond tip that moves on a (100)-diamond surface to investigate the effect of it.

This is the only case we consider in this geometry as we find that no amorphous layer arises. Only linear chains detach from the surface which cannot be quantified in terms of layers. The proposed analysis methods introduced in section 4 are not applicable.

The number of atoms contained in the simulation box shown in fig.36 is 30489 whereof 4058 atoms belong to the conical tip with a height of 7 Å, a cone radius of 7 Å at the top and 2 Å at the bottom. The tip is moved with a constant velocity of 30m/s with no force exerted on it. The bulk structure is made of 33 layers, each containing 800 diamond atoms. The eight layers at the very bottom are kept rigid, the eight layers on top of them are thermostatted by a Langevin thermostat and the atoms in the remaining 25 layers are integrated by a NVE integration.

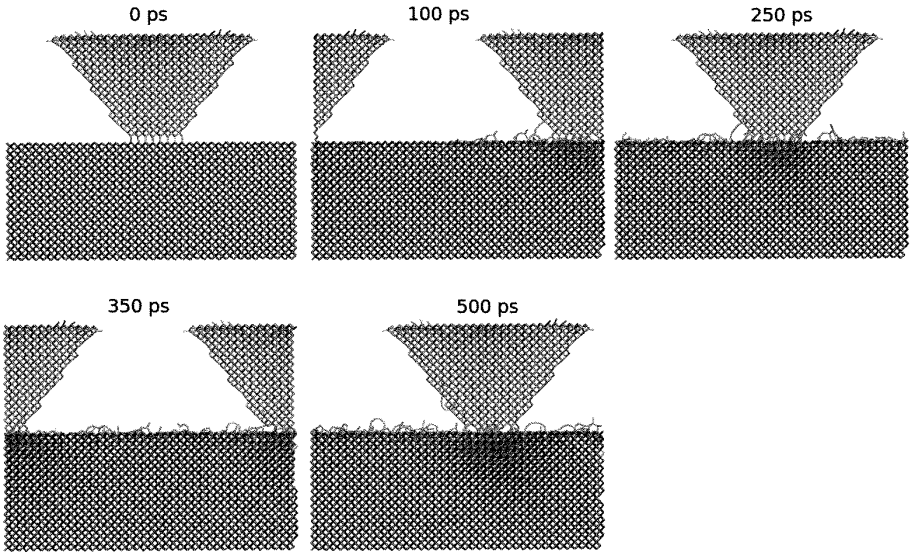

Figure 36: Snapshots after 0, 100, 250, 350 and 500 ps of the (100)-diamond tip on the (100)-diamond surface. There is no force exerted on the tip.

5.2 Surface on surface

The simulation described in section 2 is applied to several combinations of the carbon structures diamond, graphite, clathrate and the low-energy structure. The following six subsections are about pushing and sliding two carbon structures of the same kind. Later on, the results are presented for

the simulation using two different kinds of carbon structures.

In all our simulations the top layer is moved at a constant velocity of v=30m/s in the x-direction.

5.2.1 (100)-diamond with different loads

The pressure at which the (100)-diamond surfaces are pushed together is expressed as a force on the bottom rigid layer. The pressure P on a body is expressed as the normal force F, often just called load, on a surface area A.

$$P = \frac{F}{A} \tag{46}$$

We perform simulations with constant loads of 40 nN, 60 nN, 80 nN, 100 nN, 150 nN and 200 nN. The bottom rigid layer has an area of 17.78 Å by 17.78 Å.

The corresponding pressures for the values of the loads given above are 12.7 GPa, 19 GPa, 25.3 GPa, 31.6 GPa, 47.4 GPa and 63.2 GPa, respectively.

There are 3209 atoms present in the simulation box where nine of them are the adatoms placed in between the surfaces. Both bulk structures contain 1600 atoms. The 3200 atoms in total present in both bulk structures are divided into 32 layers in the z-direction which means that each layer contains 100 atoms. The dimensions of the bounding box in the x-, y- and z-direction are 17.78 Å×17.78 Å×60.46 Å.

In fig.37 the time evolution of the simulation for a pressure of 31.6 GPa (100 nN) is presented.

We see, that due to the imposed motion of the top layer in the x-direction and the pressure exerted on the bottom layer, an interface layer is created. The structure of this intermediate layer has clearly lost the crystalline order and four-fold bonding of the original diamond structure.

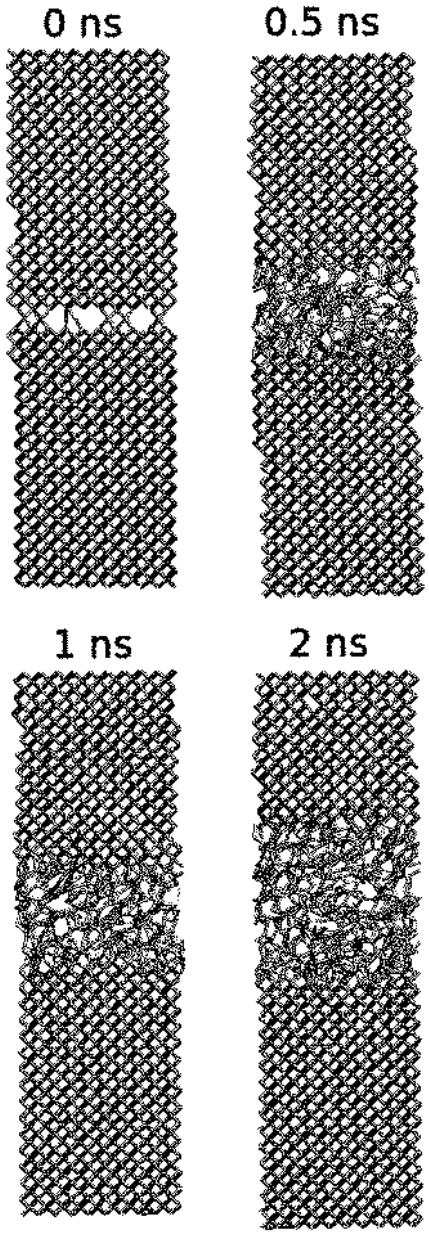

Figure 37: Snapshots after 0, 0.5, 1 and 2 ns for (100)-diamond on (100)-diamond with nine adatoms in between. The pressure between the surfaces is 31.6 GPa (100 nN exerted on the bottom layer).

In fig.38 the number of three-fold coordinated layers as a function of time is presented for different loads. The number of three-fold coordinated

layers is increasing in time signaling a change of the structure from four-fold coordinated diamond to an amorphous structure at the interface. The formation rate is higher for smaller loads.

At t=0, the number of three-fold-coordinated layers is almost zero. Looking at fig.37 it strikes that the carbon atoms at the surface are arranged zigzagways. The adatoms in between the two (100)-diamond surfaces form bonds with the surface atoms and therefore some surface atoms at the interface are three-fold-coordinated and appear in fig.37. The calculation of the coordination number is done for each atom and then normalized to the number of atoms in a single layer.

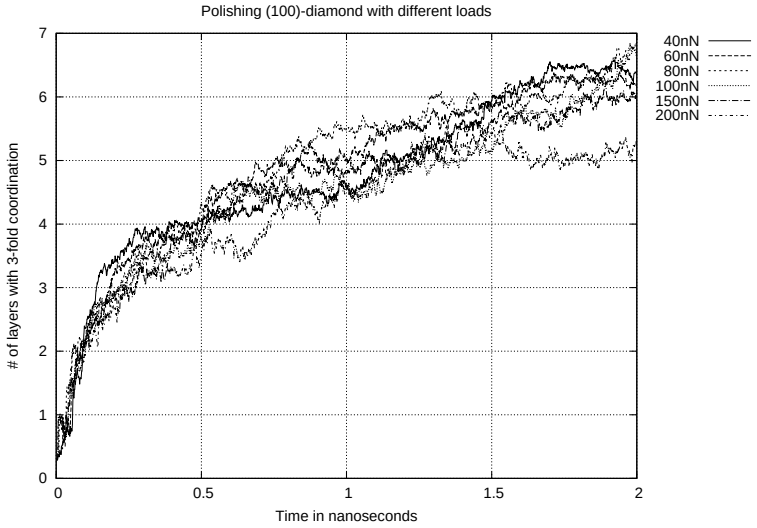

Figure 38: The number of three-fold coordinated carbon layers as a function of time at different loads is presented for the simulation of (100)-diamond shown in fig.37. The total number of layers is 32 and each layer contains 100 atoms. Notice that the formation of three-fold coordinated layers is faster at lower loads.

In fig.39 the number of four-fold coordinated layers as a function of time is presented for different loads. The number of four-fold coordinated layers is decreasing in time. The formation rate is higher for heavier loads.

There are 30 four-fold-coordinated layers at t=0 according to fig.39. This is because the carbon atoms at the top and bottom surface are two-fold-coordinated.

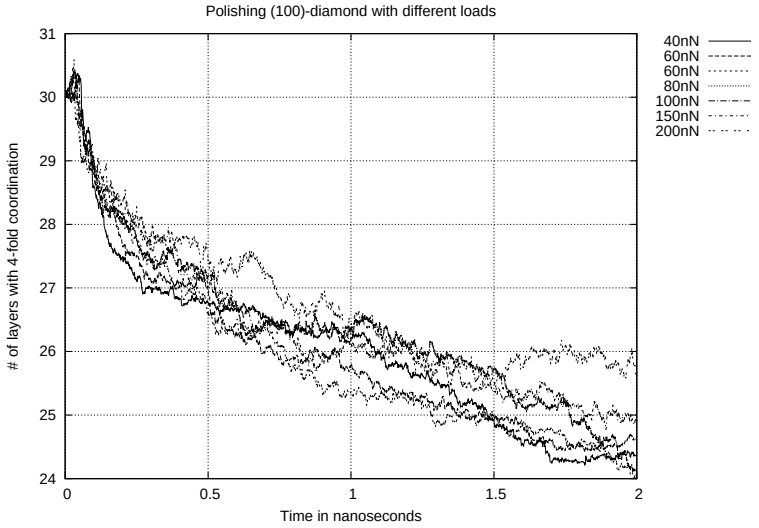

Figure 39: The number of four-fold coordinated carbon layers as a function of time at different loads is presented for the simulation of (100)-diamond shown in fig.37. The total number of layers is 32 and each layer contains 100 atoms.

Looking at both fig.38 and 39, one can see that five diamond-layers are destroyed on average and become amorphous.

The sample is divided in layers of 3 Å in the z-direction and the temperature in each of them is calculated via the equipartition theorem. In fig.40, the results for (100)-diamond is presented.

It is apparent that the highest temperature, 1800 K,is found between 30 Å and 33 Åat the interface between the bulk structures where the carbon atoms lose their long-range order and become amorphous. The temperature throughout the rest of the layers fluctuates around 600 K. The dots in the figure stand for the points in time the layers reached a certain temperature.

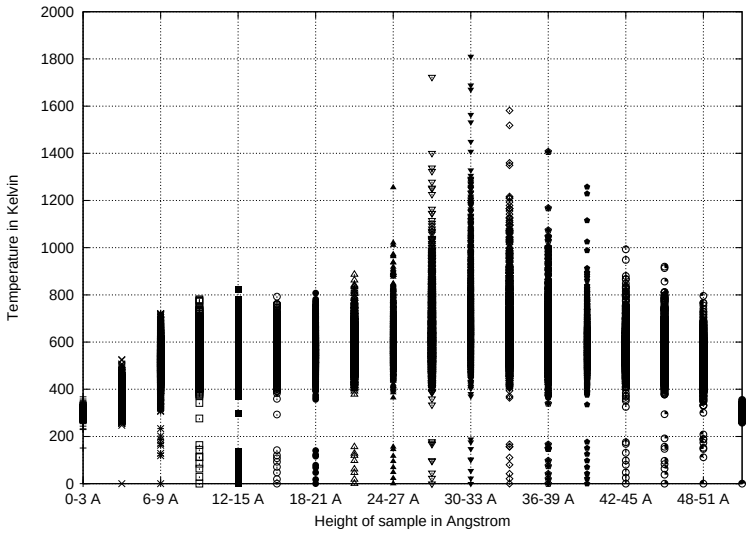

Figure 40: The simulation box of the two (100)-diamond bulk structures is divided into layers of 3 Å in the z-direction. The thermostat is set to 300 K for the top and bottom outer layers. The temperature per layer is calculated via the equipartition theorem for the simulation at 32 GPa.

The time evolution of the temperature per layer is depicted in the fig.41. The maximum temperature is reached after 1.312 ns at a height of 11·3 Å=33 Å which is roughly half of the height of the bounding box. The temperature at the interface is built up in time until it reaches its maximum at 1.312 ns and then the temperature goes down again by the end of the simulation at 2 ns. The increase in temperature occurs in the first nanoseconds where, as seen in figs. 38 and 39, many atoms change coordination and decrease when changes of the coordination occur more slowly.

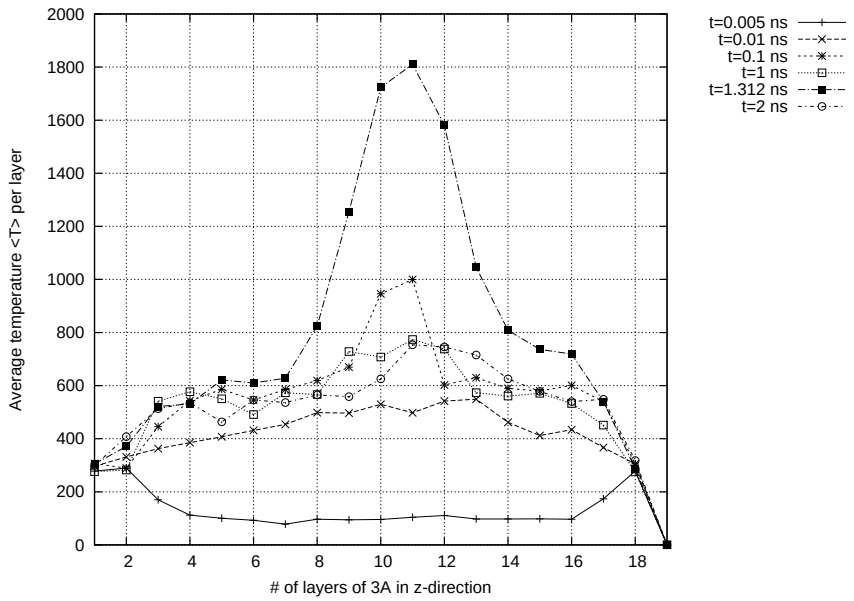

Figure 41: The temperature per layer in Kelvin in the simulation box of the two (100)-diamond bulk structures at certain instants of time.

In fig.42, the radial distribution function of the amorphous layer with z ranging from 24-42 Å is compared to the one throughout the bulk of (100)-diamond after 2 ns for the simulation performed under a pressure of 32 GPa. The radial distribution function of the amorphous layer shows two peaks, the first one at distances between 1.2 Å and 1.6 Å which is in the range of the interatomic distances for linear carbon chains up to diamond. The second peak of the solid line is broader at 2.4 Å which is roughly the distance to the second nearest neighbours for most carbon structures. The rest of the solid line fluctuates around g(r)=1 which means that the local density is equal to the average density for greater distances.

The dotted line that represents the radial distribution function throughout the bulk shows sharp peaks at 1.54 Å which is the first nearest neighbour distance, at 2.51 Å, the second nearest neighbour distance and at 2.94 Å, the third nearest neighbour distance in diamond. Many other shorter sharp peaks follow that represent the distances to the next nearest neighbours.

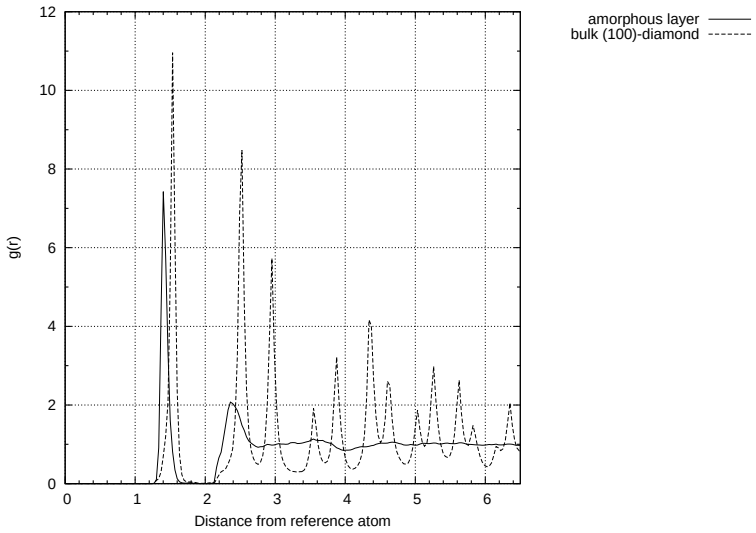

Figure 42: The radial distribution functions of the amorphous layer and the bulk at the end of the simulation of (100)-diamond (t=2 ns, F=100 nN). On the x-axis, the distance from the reference atom is given in Å and the radial distribution function g(r) as defined in section 4.1 is shown on the y-axis.

Fig.43 shows how many atoms in the amorphous layer have a certain coordination. Nearly half of all atoms are three-fold coordinated and about a quarter of them is four-fold coordinated.

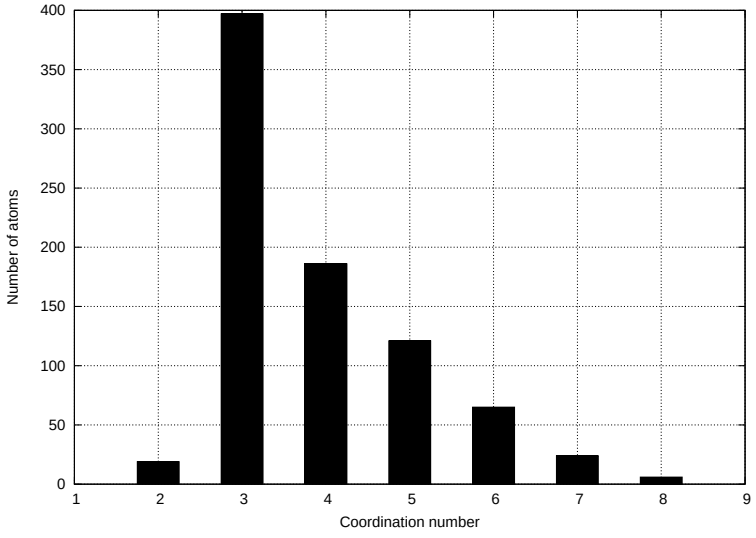

Figure 43: The coordination number for each atom in the amorphous layer at the end of the simulation of (100)-diamond is calculated (t=2ns, F=100 nN). There are 818 carbon atoms present in the amorphous layer. The cut-off distance at which the carbon atoms form a bond is set to 2.2 Å.

5.2.2 (111)-diamond with different loads

In this section we perform the same simulation as in section 5.2.1 for the system formed by (111)-diamond with constant loads of 40 nN, 60 nN, 80 nN, 100 nN, 150 nN and 200 nN. The top bottom rigid layer has an area of 20.12 Å by 21.34 Å, so the corresponding pressures are 9.3 GPa (40 nN), 14 GPa (60 nN), 18.6 GPa (80 nN), 23.3 GPa (100 nN), 35 GPa (150 nN), 46.6 GPa (200 nN).

The number of atoms in this simulation box is 4425 where nine of them do not contribute to the bulk but are placed in between the bulk structures. Each of the two bulk structures consists of 2208 atoms, thus altogether there are 4416 bulk atoms. The structure is divided into 46 layers in the z-direction. Each layer contains 96 atoms. The dimensions of the bounding box in the x-, y- and z-direction are 20.12 Å×21.34 Å×60.72 Å.

In fig.44 the time evolution of the simulation for a pressure of 23.3 GPa (100 nN) is presented.

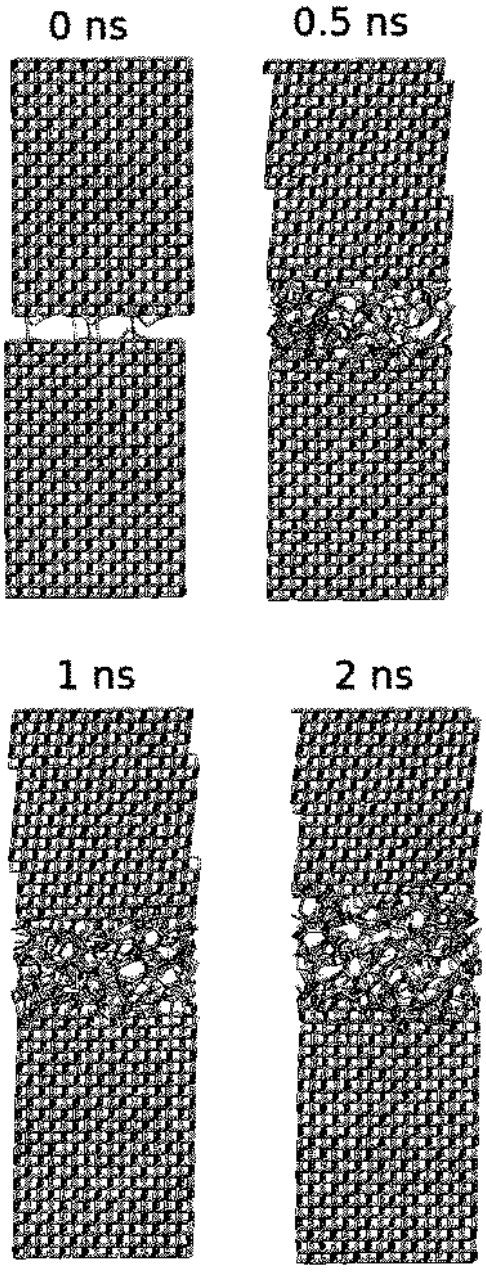

Figure 44: Snapshots after 0, 0.5, 1 and 2 ns for (111)-diamond on (111)-diamond with nine adatoms in between. The pressure between the surfaces is 23 GPa (100 nN exerted on bottom layer).

At t=0, fig.45 displays that the number of three-fold-coordinated layers is almost four. This is due to the fact that the carbon atoms at the four surfaces

(see fig.44) are three-fold-coordinated as no periodic boundary conditions are applied in the z-direction. Nine adatoms are placed at the interface between both bulk structures. They form bonds with the surface atoms. As already mentioned, the calculation of the coordination number is performed for each atom and then normalized to the number of atoms in a layer. That is why fig.45 shows that the number of three-fold-coordinated layers is not exactly four.

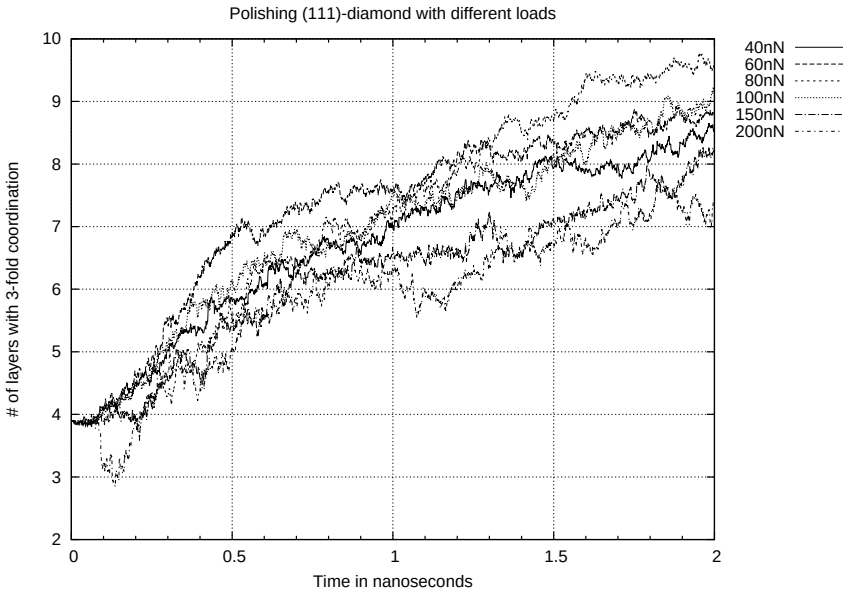

Figure 45: The number of three-fold coordinated carbon layers as a function of time at different loads is presented for (111)-diamond. The total number of layers is 46 with 96 atoms per layer. Notice that the formation of three-fold coordinated layers is faster at lower loads.

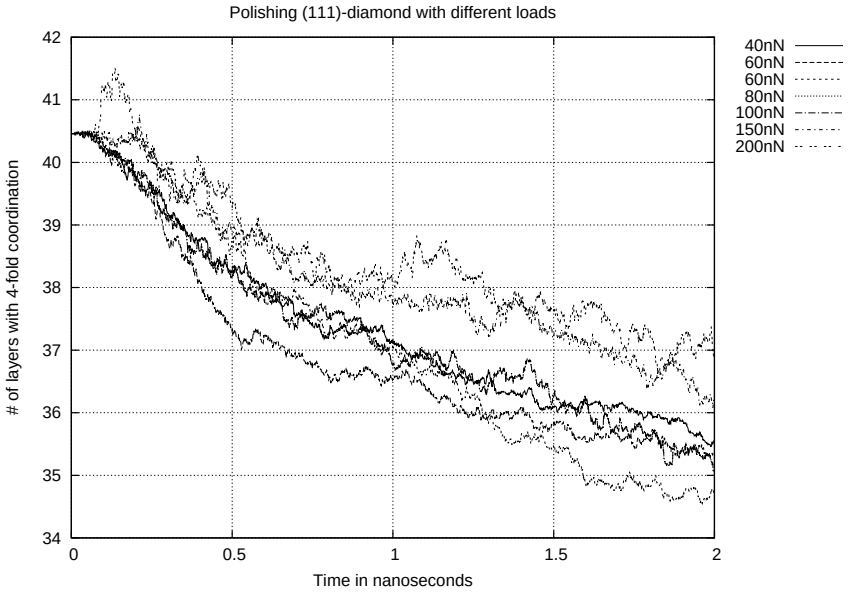

Figure 46: The number of four-fold coordinated carbon layers as a function of time at different loads is presented for (111)-diamond. The total number of layers is 46.

Looking at both fig.45 and 46, one can see that four diamond-layers are destroyed on average and become amorphous. Comparing these figures to figures 38 and 39, one can state that more layers are destroyed for (100)-diamond.

The sample is again divided in layers of 3 Å in the z-direction and the temperature in each of them is calculated via the equipartition theorem. In fig.47, the results for (111)-diamond is presented. The same observations as made for the (100)-diamond simulation (see previous section 5.2.1), can be made here. The highest temperature is 1500 K reached at a height between 33 Å and 36 Å. Throughout the rest of the layers the temperature fluctuates between 600 K and 800 K. In comparison to fig.40 obtained for the (100)-diamond simulations, the temperatures for (111)-diamond are about 200 K lower.

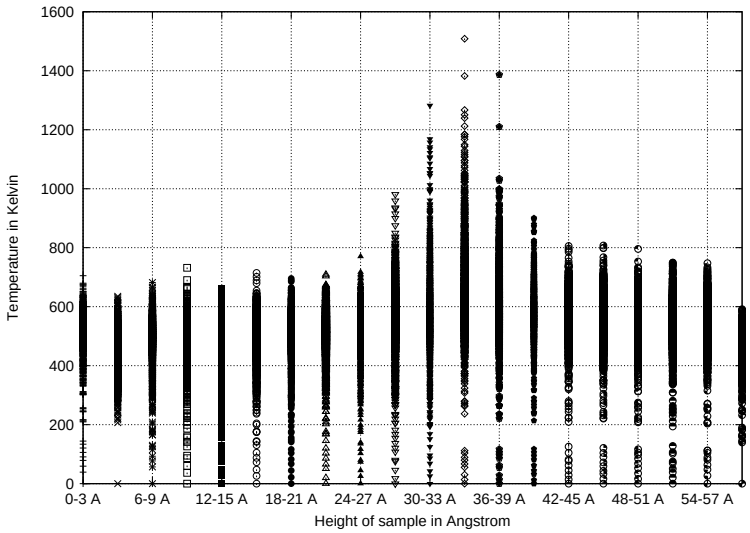

Figure 47: The simulation box is divided into layers of 3 Å in the z-direction. The thermostat is set to 300 K. The temperature per layer is calculated via equipartition (see section 4.3) for the simulation of (111)-diamond at 23 GPa.

The time evolution of the temperature per layer is depicted in the fig.48. The highest temperature is reached after 1.87 ns at in layer number 12 which is at a height between 33 Å and 36 Å. This is at the interface of the two bulk structures and is an indication therefore that the atoms move their a lot. Their movement is so strong that they have to leave their position in the lattice.

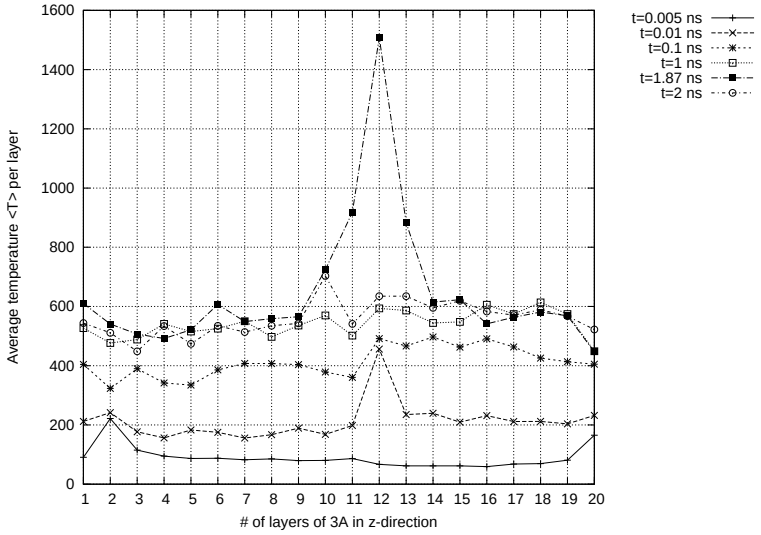

Figure 48: The temperature per layer in Kelvin in the simulation box of the two (111)-diamond bulk structures at certain instants of time.

The radial distribution function is again calculated for the amorphous layer and the bulk for the (111)-diamond simulation just as it was done for the (100)-diamond simulation (see section 5.2.1). The figure can be discussed the same way as done for the (100)-diamond simulation. They are very similar.

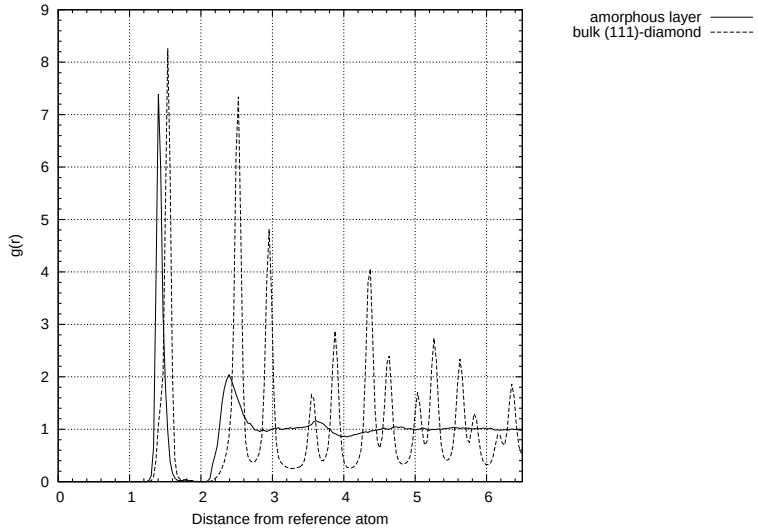

Figure 49: The radial distribution function of the amorphous layer and the bulk at the end of the simulation of (111)-diamond (t=2ns, F=100 nN). On the x-axis, the distance from the reference atom is given in Å and the radial distribution function g(r) as defined in section 4.1 is shown on the y-axis.

Nearly half of the atoms in the amorphous layer are three-fold coordinated and only about one fifth of them is four-fold coordinated (see fig.50). Compared to fig.43 for the (100)-diamond simulation, there are less four-fold coordinated atoms present in this one.

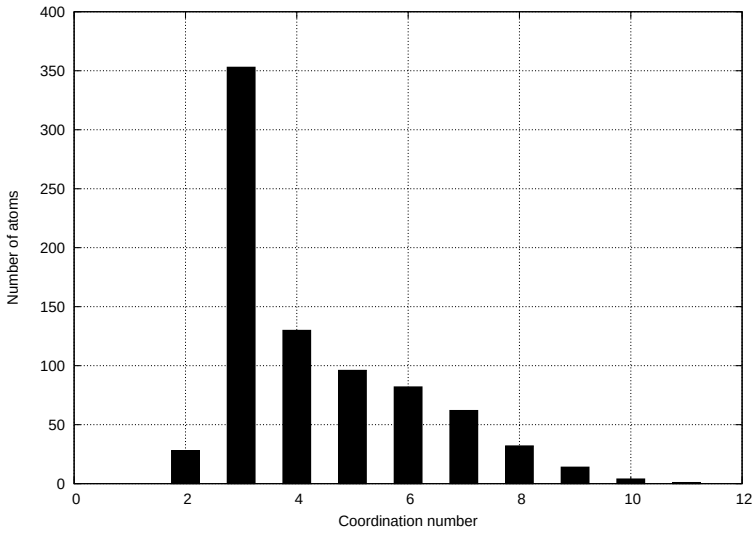

Figure 50: The coordination number for each atom in the amorphous layer at the end of the simulation of (111)-diamond is calculated (t=2ns, F=100 nN). There are 802 carbon atoms present in the amorphous layer. The cut-off distance at which the carbon atoms form a bond is set to 2.2 Å.

5.2.3 Graphite

The bounding box presented in fig.51 contains 17 layers each with 176 atoms. In total, there are 3001 atoms whereof nine are adatoms between the two graphitic bulk structures. The dimensions of the bounding box in the x-, y- and z-direction are 19.90 Å×21.36 Å×64.24 Å.

Looking at fig.51, it strikes that graphitic bulk structures are not destroyed even though here the pressure is 190 GPa, about five times higher than the ones presented for (100) and (100)-diamond. The top six layers are bent which might be a result from the force exerted on the top layer. Apart from that, the graphitic structures do not change.

The outcome might have been different if we had considered an even higher pressure was higher as we do for the simulation of incommensurate graphite in the next section 5.2.4. Then, the graphite structure would experience a high enough pressure to become (100)-diamond and to build up an amorphous layer at the interface.

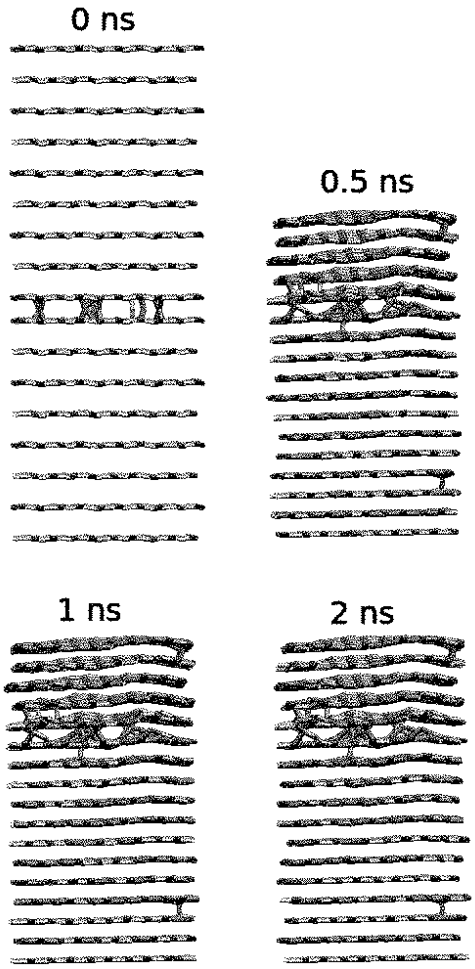

Figure 51: Snapshots after 0, 0.5, 1 and 2 ns for graphite. The pressure between the surfaces is 190 GPa.

In fig.52, the coordination number per layer is calculated. The simulation box is therefore divided into layers of 1.5 Å in the z-direction and the average coordination number per layer is calculated. The dots represent points in time.

It strikes that the coordination number fluctuates around the value 3 which means that some atoms lose or make additional bonds to other atoms due to the compression of the layers. However, it is not enough to see a significant change in the structure.

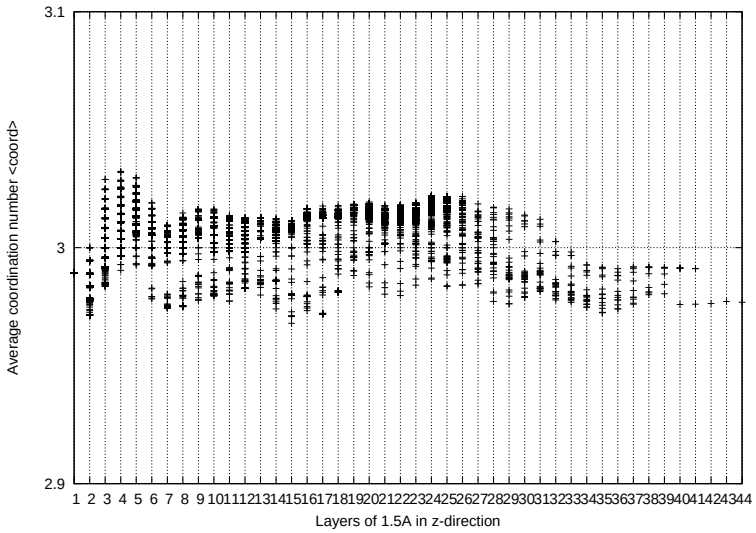

Figure 52: The simulation box is divided into layers of 1.5 Å in the z-direction. The coordination number per layer is calculated for the simulation of graphite at 190 GPa.

5.2.4 Incommensurate graphite

In fig.53, the bounding box for incommensurate graphite is shown that has 6720 atoms in total. Beginning from the bottom, it is made up by twelve layers of graphite. The upper nine layers are rotated by 30 °. Each layer contains 336 atoms. The dimensions of the bounding box in the x-, y- and z-direction are 29.82 Å×29.82 Å×66.91 Å.

It can be seen from fig.53 that the pressure of 484 GPa is high enough in order to see a transformation from graphite at the bottom layers to (111)-diamond and to (111)-diamond rotated by 30 ° at the top.

Presumably the pressure should have been higher in order to achieve the formation of an amorphous layer.

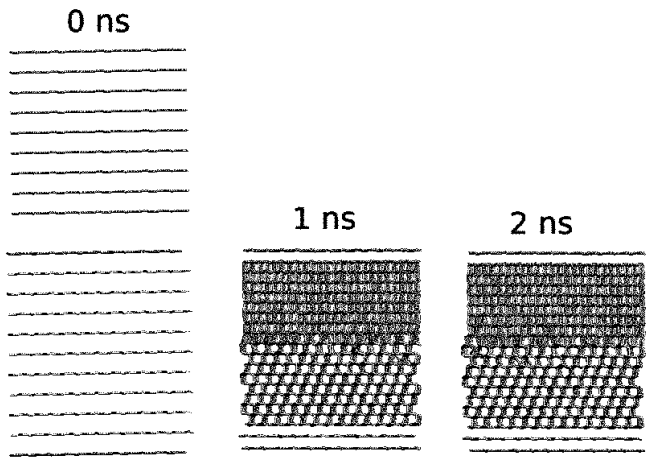

Figure 53: Snapshots after 0, 1, and 2 ns for incommensurate graphite. The pressure between the surfaces is 484 GPa.

In the next fig.54 the coordination per layer is calculated. Especially the atoms at the bottom layers experience a transformation from a three-fold to a four-fold coordination. According to the figure, the top layers do not show a clear transformation from a three- to a four-fold coordination.

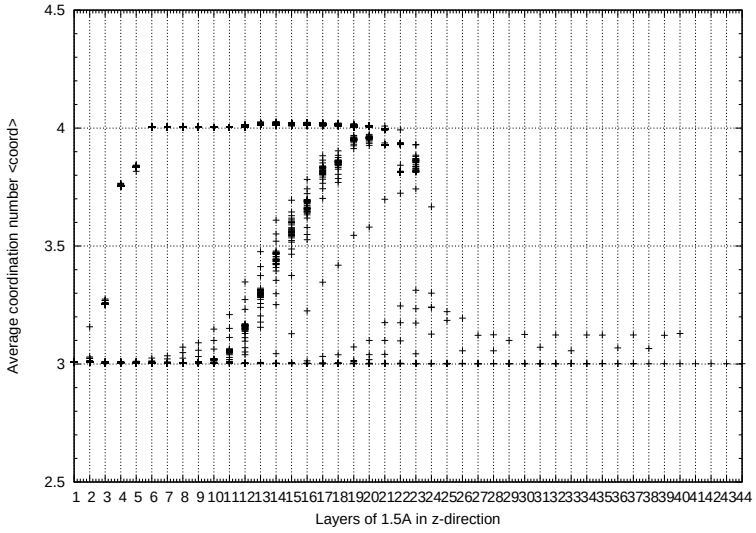

Figure 54: The simulation box is divided into layers of 1.5 Å in the z-direction. The coordination number per layer is calculated for the simulation of incommensurate graphite at 484 GPa.

It would be interesting to see in more detail if there is an effect of the stacking in graphite from the AB Bernal stacking considered in section 5.2.3

to the incommensurate case shown in this section.

5.2.5 Clathrate

The simulation box as presented in fig.55 contains 744 atoms. Eight atoms are placed between the clathrate structures. Both structures are made up by two layers of cages, each layer containing 184 atoms. We remind that bulk clathrates are fully four-fold coordinated. The dimensions of the bounding box in the x-, y- and z-direction are 12.79 Å×12.20 Å×28.85 Å. It is the smallest bounding box that is made in our series of simulations.

In fig.55, the time evolution of the simulation is shown. It is obvious that the simulation box is chosen too small and the Langevin layer too thick compared to the total height of the sample. Therefore the clathrate structures are destroyed in a short period of time.

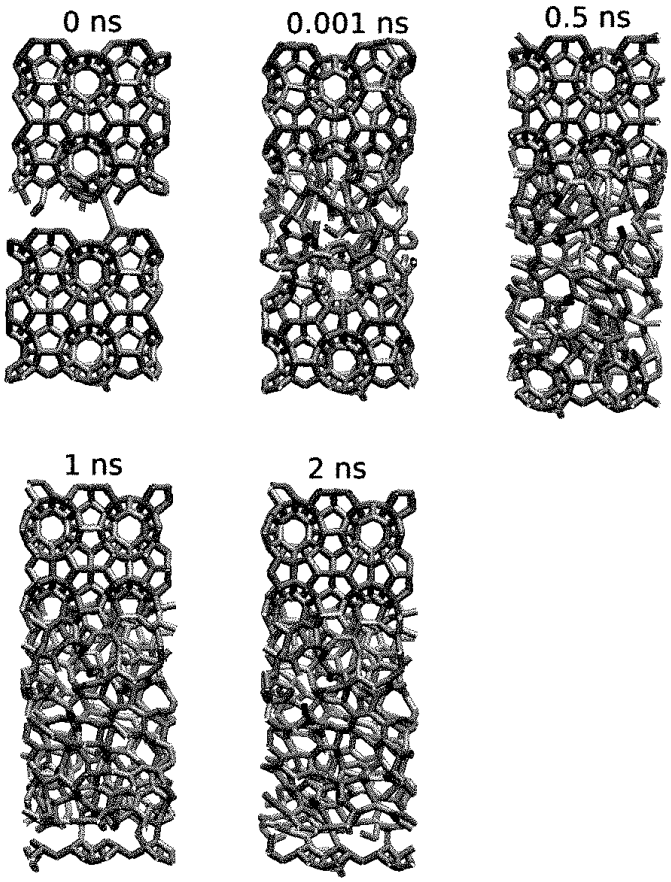

Figure 55: Snapshots after 0, 0.001, 0.5, 1 and 2 ns for clathrate. The pressure between the surfaces is 0.1 GPa.

Fig.56 shows the coordination number per layer. For the upper part of the simulation box, the coordination number fluctuates between three and four. The bottom part of the clathrate structure is destroyed the most. There, the coordination number fluctuates between 3 and 3.5 which means that most atoms underwent a transformation to a three-fold coordination. Some still remained four-fold coordinated but not enough to demonstrate a significant change.

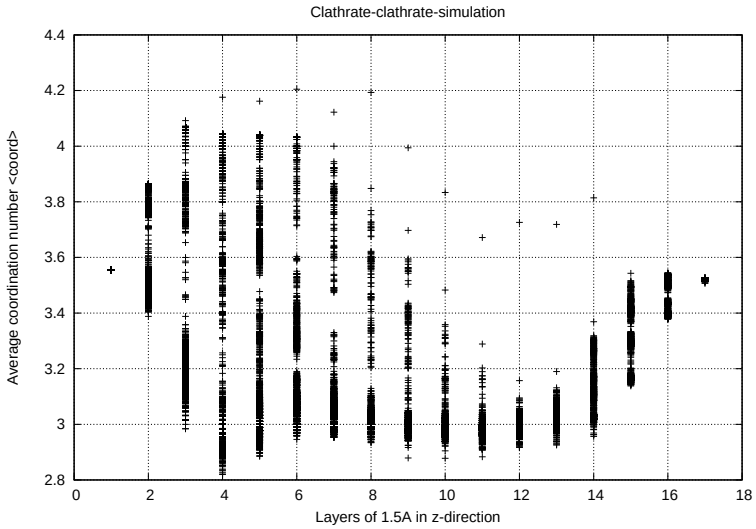

Figure 56: The simulation box is divided into layers of 1.5 Å in the z-direction. The coordination number per layer is calculated for the simulation of clathrate at 0.1 GPa.

5.2.6 Low-energy structure

This simulation box contains 9025 atoms whereof nine are adatoms between the low-energy structures. The bottom low-energy structure consists of twelve layers of 392 atoms and the top one is made up by eleven layers of 392 atoms. The dimensions of the bounding box in x-, y- and z-direction are 32.79 Å×30.41 Å×56.22 Å.

In fig.57 the formation of an amorphous layer is observed. It becomes thicker as the time goes by.

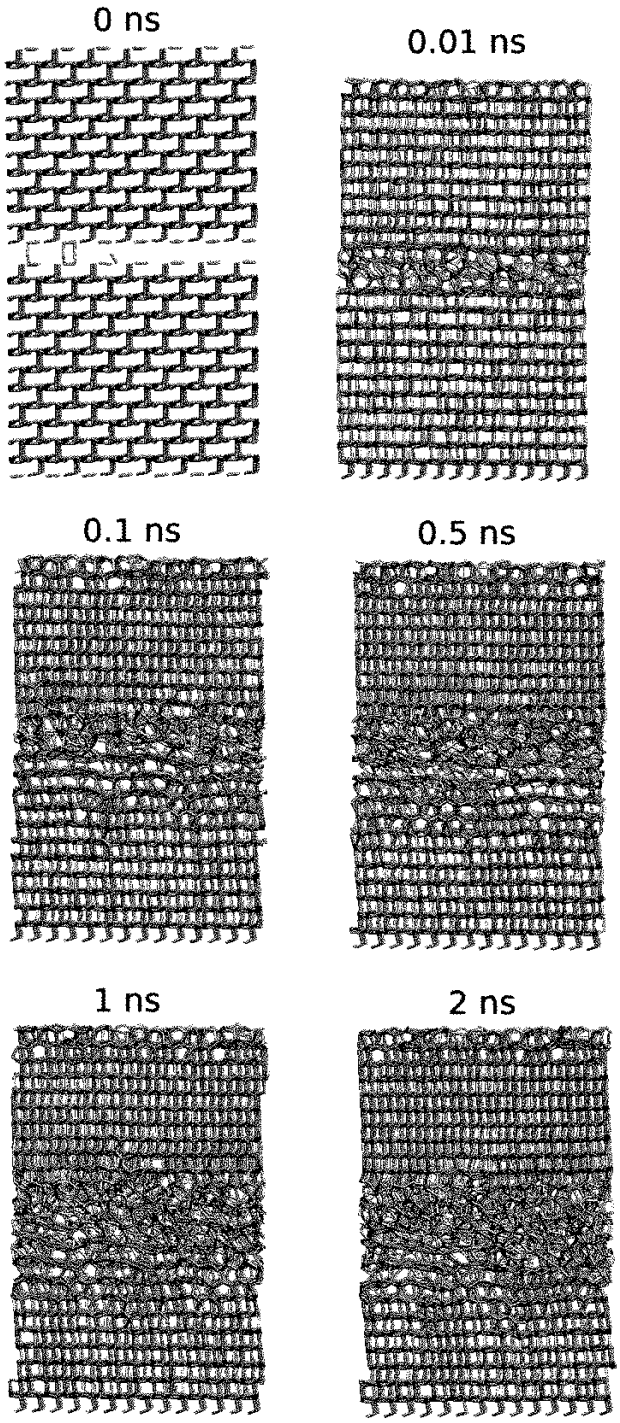

Figure 57: Snapshots after 0, 0.01, 0.1, 0.5, 1 and 2 ns for the low-energy structure. The pressure between the surfaces is 63 GPa.

Fig.58 shows the coordination number per layer. The dots represent points in time. At the very top and bottom of the simulation box the coordination number is four. Approaching the interface, the atoms become three-fold-coordinated.

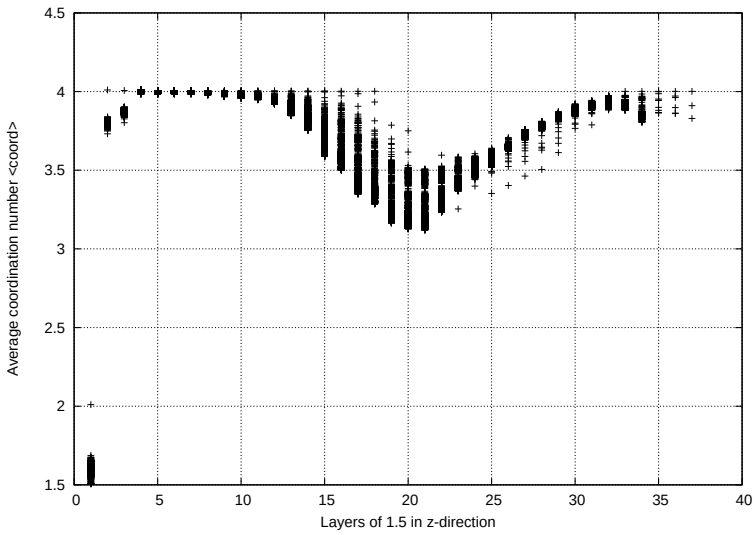

Figure 58: The simulation box is divided into layers of 1.5 Å in the z-direction. The coordination number per layer is calculated for the simulation of the low-energy structure at 63 GPa.

5.2.7 (111)-diamond on graphite

The simulation explained in section 2 is applied to the simulation box depicted in fig.59. There are 6393 carbon atoms present in the simulation box, where nine of them are adatoms. There are nine layers of graphite (in the AB Bernal stacking) each of them containing 280 carbon atoms and 23 layers in diamond, each consisting of 168 atoms. The dimensions of the bounding box in the x-, y- and z-direction are 30.18 Å×24.89 Å×60.85 Å.

Fig.59 shows the snapshots after 0, 5, 10 and 20 ns. The pressure is not high enough to observe a significant change for both structures. The compression of the structures leads to a few additional bonds for some atoms.

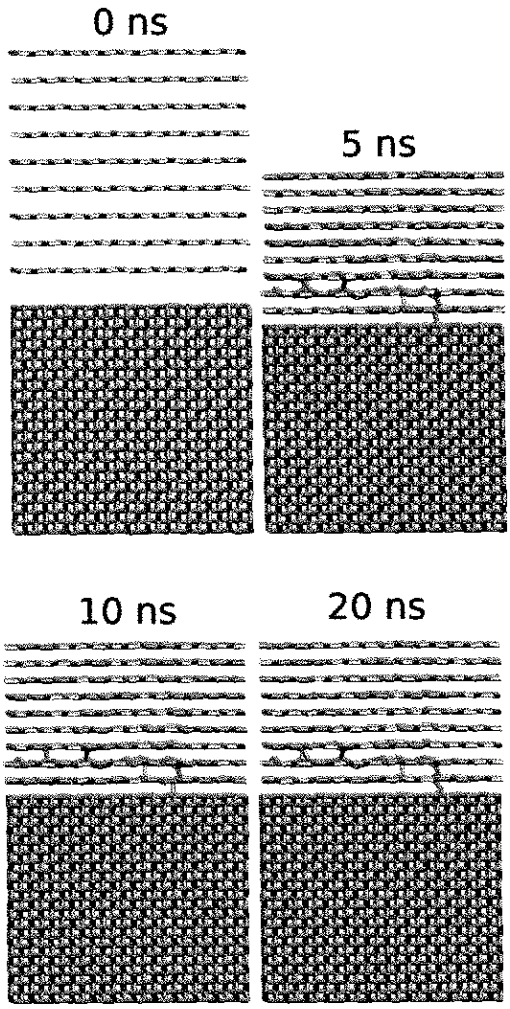

Figure 59: Snapshots after 0, 5, 10 and 20 ns for graphite on (111)-diamond. The pressure between the surfaces is 150 GPa.

The temperature per layer is shown in fig.59. The temperature does not change dramatically throughout the sample. The temperature fluctuates around 400 K and only the layers 10, 11 and 16 deviate from that reaching temperatures of up to 550 K (layer 11).

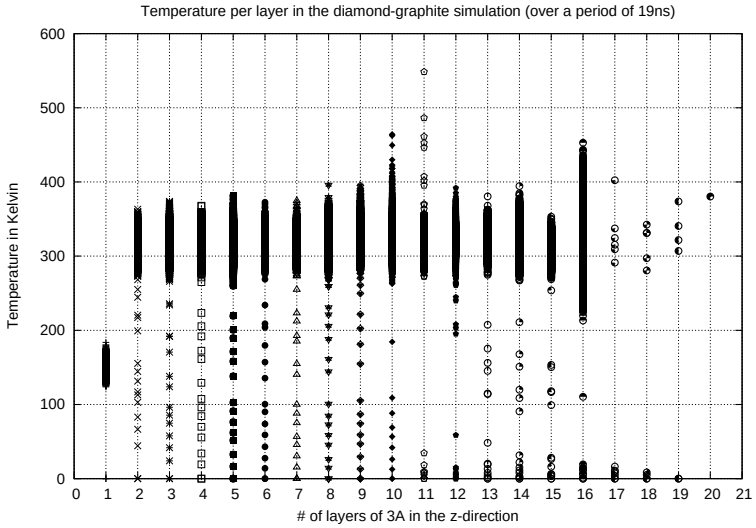

Figure 60: The simulation box is divided into layers of 3 Å in the z-direction. The temperature per layer is calculated via equipartition (see section 4.3) for the simulation of graphite on (111)-diamond at 150 GPa.

The coordination number per layer is shown in fig.60. Diamond at the bottom of the simulation box is clearly four-fold coordinated and graphite at the top is three-fold coordinated. The graphitic layers are compressed in such a way that the interlayer distance is small enough for a few carbon atoms to form a fourth bond (see fig.59). That is why the coordination number of the atoms close to the interface between graphite and (111)-diamond fluctuates between four and three.